



## Multi - Target Detection Capability of Linear Fusion Approach under Different Swerling Models of Target Fluctuation

By Mohamed Bakry El\_Mashade

*Al Azhar University*

**Abstract-** In evolving radar systems, detection is regarded as a fundamental stage in their receiving end. Consequently, detection performance enhancement of a CFAR variant represents the basic requirement of these systems, since the CFAR strategy plays a key role in automatic detection process. Most existing CFAR variants need to estimate the background level before constructing the detection threshold. In a multi-target state, the existence of spurious targets could cause inaccurate estimation of background level. The occurrence of this effect will result in severely degrading the performance of the CFAR algorithm. Lots of research in the CFAR design have been achieved. However, the gap in the previous works is that there is no CFAR technique that can operate in all or most environmental varieties. To overcome this challenge, the linear fusion (LF) architecture, which can operate with the most environmental and target situations, has been presented.

**Keywords:** *adaptive detection, non-coherent integration, fluctuating targets, swerling models, target multiplicity environments.*

**GJCST-H Classification:** I.5.1



MULTITARGETDETECTIONCAPABILITYOFLINEARFUSIONAPPROACHUNDERDIFFERENTSWERLINGMODELSTARGETFLUCTUATION

*Strictly as per the compliance and regulations of:*



# Multi -Target Detection Capability of Linear Fusion Approach under Different Swerling Models of Target Fluctuation

Mohamed Bakry El\_Mashade

**Abstract-** In evolving radar systems, detection is regarded as a fundamental stage in their receiving end. Consequently, detection performance enhancement of a CFAR variant represents the basic requirement of these systems, since the CFAR strategy plays a key role in automatic detection process. Most existing CFAR variants need to estimate the background level before constructing the detection threshold. In a multi-target state, the existence of spurious targets could cause inaccurate estimation of background level. The occurrence of this effect will result in severely degrading the performance of the CFAR algorithm. Lots of research in the CFAR design have been achieved. However, the gap in the previous works is that there is no CFAR technique that can operate in all or most environmental varieties. To overcome this challenge, the linear fusion (LF) architecture, which can operate with the most environmental and target situations, has been presented. This processor is a combination of the properties of three different CFAR algorithms (CA, OS, and TM), and forms two different processes: statistical ordering and averaging. This paper is devoted to analyze LF structure when the primary and the secondary targets are considered to be fluctuating in terms of four Swerling models. Closed-form expression is derived for the processor performance. Superiority of the LF algorithm over the conventional ones in multi-target scenarios is verified by numerical simulation. Additionally, the LF ideal performance outperforms that of Neyman-Pearson (N-P) detector, which is the basic reference in the CFAR world. Moreover, the LF detector mitigates the impact of outlying targets and has the capability of holding the rate of false alarm stationary in face of outliers.

**Keywords:** adaptive detection, non-coherent integration, fluctuating targets, swerling models, target multiplicity environments.

## I. INTRODUCTION

Radar systems are widely used for safety purposes. For case in point, they are utilized at airports to safely regulate the air traffic and in a military context, they are employed to defend against hostile missiles. The mission of the radar is to detect targets of interest and to discard those that don't concern a particular application.

Depending on the type of radar application, the system might be concerned with estimating the target radar cross section (RCS), measuring and tracking its

position or velocity, imaging it, or providing fire control data to direct weapons to the target. In all of these practical applications, one of the most fundamental tasks of a radar is the detection; the process of examining the radar data and determining if it represents interference only, or interference plus echoes from a target of interest (ToI) [1-5].

The detection capability is one of the most significant factors in the behavior of such type of vital systems. Normally, the purpose of detection is to distinguish genuine target reflections from noise and clutter. More specifically, target detection can be regarded as a style of classification, which distinguishes whether the tested signal contains an echo from a target or just corresponds to the noise. This process relies on the thresholding criteria. This criteria has two philosophies: fixed and adaptive. Although the fixed threshold is simple in design, it has a misdetection and this procedure deprives the system from its ability to control the false alarm rate. This strategy of detection is useful for non-fluctuating targets of identical reflection models but fails when a mixture of different targets exists in radar's field of view (FoV). Therefore, variable threshold will be needed to cover such scenarios. For this reason, adaptive detection thresholds have been the subject of research for a long time. In other words, there is a demand for a detection process that is based on dynamic, instead of static, threshold to cope with those situations of inhomogeneous or changing clutter environment all over the search space. This is the objective of the second philosophy. Constant false alarm rate (CFAR) technology is the most popular target detection framework to address the issues associated with fixed threshold. This technology is crucial as a desired property for automatic target detection in an unknown and non-stationary background. In other words, CFAR is a property that is assigned to the processor in which the threshold, or gain control devices, guarantees an approximately constant rate of false target detection when the noise/clutter level temporally varies. The feature of CFAR activates the threshold in such a way that it becomes adaptive to the local clutter environment. Thus, the CFAR mechanism maintains the amount of false alarm under supervision in a diverse background of interference. It should be taken into account that this approach doesn't come at no cost.





failing to recognize a signal (miss probability) or falsely indicating the presence of a signal (false alarm probability). On the other hand, to cope with a changing clutter environment, there is a persistent need of dynamic and adaptive threshold. This threshold must be varied, up and down, in accordance with the background level for the false alarm rate to be maintained at its pre-set value. A detector with this characteristic is designated as constant CFAR. Thus, the CFAR strategy is the main goal of the radar system designer.

For the CFAR circuit to be efficient, it must realize some characteristics. The more motivating features include rigorous fitting of the detection threshold to the clutter background, masking avoidance of closely spaced targets, low CFAR loss, and constructing a threshold that gives point as well as extended targets the chance to pass. Whatever the structure of the CFAR model is, the framework of sliding window is regarded as its basic arrangement. As Fig.(1) depicts, this window moves throughout the coverage area, and contains a set of reference cells (RC's) around the central cell, which is termed as cell under test (CUT). To alleviate self-interference in a real target echo, some guard cells (GCs) embrace CUT. These cells are used as buffer between CUT and the training cells. They are excluded from the background computation to insure that the CUT doesn't affect the threshold calculation. The declaration of the presence of a target is carried out if the power of CUT is greater than the power of both GCs and the estimated level. Each resolution cell has the chance to occupy the position of CUT. In this regard, the RC's that have been already processed constitute the leading subset, whilst those that have not yet occupied the center organize the lagging subset. The size selection of the sliding window is dependent upon rugged knowledge of the typical clutter background. Generally, the window length  $N$  should be as large as possible for the estimation process to be of good modality. Meanwhile,  $N$  is preferred to be compatible with the typical range extension of homogeneous clutter zones for the demand of identically distributed random variables to be statistically satisfied. Normally, the typical value of  $N$  lies in the 16-32 range.

The detection threshold is established as the product of the estimated noise power  $Z$  by a scaling factor  $T$ , which is imposed to verify the desired rate of false alarm, as Fig.(1) portrays. By comparing the content of CUT with the resulting threshold, the procedure will recommend that the signal is belonging to a target, if the magnitude of the CUT surpasses the calculated threshold. Otherwise, the signal is coming from interference and no target is present.

Most modern radar systems are of coherent type. This means that they receive the returned signal in a polar (amplitude and phase) form. In the radar

receiver, the synchronous detector generates an in-phase ( $I$ ) and a quadrature ( $Q$ ) components from the received signal. Whilst the in-phase component denotes the real part, the quadrature component represents the imaginary part of the received signal. Under the null hypothesis ( $H_0$ ), the received noise for both  $I$  and  $Q$  channels is modeled as an independent and identically distributed (IID) Gaussian random process with zero mean and of variance  $\psi/2$ . In addition,  $I$  and  $Q$  channels are statistically independent. Thus, the received noise is a complex Gaussian signal ( $N=I+iQ$ ) with  $\mu=0$  and  $\sigma_n^2=\psi$ .

After pulse compression, the signal passes through a rectifier, which converts the complex signal into an amplitude and phase. In this vein, there are two familiar types of rectifiers: linear and square-law detectors. The linear detector measures only the magnitude  $(I^2+Q^2)^{1/2}$  of the complex received signal, which follows the Rayleigh distribution. The square-law detector, on the other hand, measures only the power  $(I^2+Q^2)$  of the linear detector, the distribution of which is exponential. For both types, the phase is uniformly distributed in the interval  $[-\pi, \pi]$  [17].

#### a) Neymann - Pearson Detector

The Neyman-Pearson (N-P) processor operates with a detection threshold which is imposed in such a way that for a desired rate of false alarm, the level of detection will be maximized. This threshold is fixed and is derived from a known interference PDF. Practically, the using of N-P detector necessitates: 1) the background interference is IID over all resolution cells, to which the fixed threshold is to be applied, 2) the interference is of statistical distribution the parameters of which are known, 3) the interference environment is homogenous.

Generally, the detection process is achieved at the output of the rectifier and yields one of three possible outcomes: correct decision, missed detection, or false alarm. A correct decision is one in which the detector correctly declares the presence/absence of a target. A missed detection is one in which the detector declares the absence of a target when in truth the measurement contains a target return. A false alarm occurs when the detector declares the presence of a target and in reality a target's return is not present in the measured data. Whilst the first outcome is specified by  $P_d$ , the second one represents its complement  $(1 - P_d)$ . Therefore,  $P_d$  plays an important role in determining the first two outcomes. The last outcome is characterized by  $P_{fa}$ . Thus, once  $P_d$  and  $P_{fa}$  are calculated, the processor performance is completely evaluated.

Here, we are concerned with square-law type of signal rectifiers. Thus, as we have noted above, the square-law detected output for any range cell ( $v_0$ ) has an exponential distribution, the general formulation of which is:

$$p_{v_0}(v) = \frac{1}{\eta} \exp\left(-\frac{v}{\eta}\right) U(v) \quad (1)$$

In the above expression,  $U(\cdot)$  stands for the unit-step function. The value of  $\eta$  depends on the situation of operation and can take one of the following values:

$$\eta \triangleq \begin{cases} \psi & \text{for} & \text{Clear Background} \\ \psi(1 + \gamma) & \text{for} & \text{Object Under Test} \\ \psi(1 + \theta) & \text{for} & \text{Spurious Background} \end{cases} \quad (2)$$

In the preceding formula, " $\gamma$ " denotes the signal-to-noise ratio (SNR) of the Tol return, whereas " $\theta$ " symbolizes the interference-to-noise ratio (INR) of the interfering target return, and " $\psi$ " represents the background noise power.

$$P_s = \int_{Tr}^{\infty} \frac{1}{\eta} \exp\left(-\frac{v}{\eta}\right) dv = 1 - F_{v_0}(Tr) \quad (3)$$

It may be rarely that a decision is made on the basis of a single transmitted pulse. More often, a lot of pulses are transmitted, and the resulting received signal is integrated or processed in some way to enhance, relative to the mono-pulse case, the SNR. In this regard,

$$p_{v_0}(v) = \left(\frac{1}{\eta}\right)^M \frac{v^{M-1}}{(M-1)!} \exp\left(-\frac{v}{\eta}\right) U(v) \quad (4)$$

The cumulative distribution function (CDF) corresponding to the PDF of Eq.(4) has a form given by:

$$F_{v_0}(v) = 1 - \sum_{\ell=0}^{M-1} \frac{(v/\eta)^\ell}{\ell!} \exp\left(-\frac{v}{\eta}\right) U(v) \quad (5)$$

In radar systems, detection performance is always related to target models and background environments. Thus, the availability of the statistical characteristics of a target's radar cross-section (RCS) can significantly ameliorate the performance of the detection algorithm. For this purpose, Swerling

$$p_{v_0}(v/\bar{\gamma}) = \left(\frac{\kappa}{\gamma + \kappa}\right)^\kappa {}_1F_1\left(\kappa; M; \frac{\bar{\gamma}}{\gamma + \kappa} v\right) \frac{v^{M-1}}{(M-1)!} e^{-v} U(v) \quad (6)$$

${}_1F_1(\cdot)$  stands for the confluent hyper-geometric function and  $\bar{\gamma}$  denotes the average M-pulse SNR. The calculation of the CDF associated with this PDF yields:

$$F_{v_0}(v) = \zeta^\kappa \sum_{j=0}^{\infty} \frac{(\kappa)_j}{j!} (1 - \zeta)^j \left\{ 1 - \sum_{\ell=0}^{M+j-1} \frac{v^\ell}{\ell!} e^{-v} \right\} \quad \& \quad \zeta \triangleq \frac{\kappa}{\gamma + \kappa} \quad (7)$$

with

$$\kappa = \begin{cases} 1 & \text{for} & SWI \\ M & \text{for} & SWII \\ 2 & \text{for} & SWIII \\ 2M & \text{for} & SWIV \\ \infty & \text{for} & SWV \end{cases} \quad (8)$$

and

$$(\kappa)_j \triangleq \frac{\Gamma(\kappa + j)}{\Gamma(\kappa)} = \begin{cases} 1 & \text{if } j = 0 \\ \kappa(\kappa+1)(\kappa+1)\dots\dots(\kappa + j - 1) & \text{if } j > 0 \end{cases} \quad (9)$$

The substitution of Eq.(7) into Eq.(3) and using the values indicated in Eq.(8), the N-P performance can be easily obtained for fluctuating targets of different Swerling's models.

b) *Constant False Alarm Rate (CFAR) Detector*

CFAR detectors are designed to track changes in the interference and to adjust the detection threshold to maintain a constant probability of false alarm. Since the performance of a detection scheme is measured by

$$P_d \triangleq \Pr\left(Z \left\langle \frac{v_0}{T} \right\rangle \middle| H_1\right) = \int_0^{\infty} p_{v_0}(x) \int_0^{v_0/T} p_z(y) dy dx = T \int_0^{\infty} p_{v_0}(Tv) F_z(v) dv \quad (10)$$

$F_z(\cdot)$  denotes the CDF of the noise power level estimate and  $T$  is a thresholding constant required to guarantee the designed rate of false alarm. In terms of the Laplace transformation, Eq.(10) takes the form:

$$P_d = T \left. \Phi_g(\Omega) \right|_{\Omega=0} \quad \text{with} \quad \Phi_g(\Omega) \triangleq \int_0^{\infty} p_{v_0}(Tv) F_z(v) \exp(-\Omega v) dv \quad (11)$$

With the aid of convolution theorem, Eq.(11) can be put in another form as:

$$\Phi_g(\Omega) = \frac{1}{T} M_{v_0}(\Omega/T) * \Theta_z(\Omega) \quad (12)$$

In the above formula,  $M_x(\cdot)$  represents the moment generating function (MGF) of the random variable (RV)  $x$ ,  $\Theta_z(\cdot)$  denotes the Laplace transformation of the CDF of the RV  $Z$ , and the symbol "\*" stands for the convolution process. By using Eq.(12), Eq.(10) can be written as:

$$P_d = \frac{1}{2\pi j} \oint_{C^-} M_{v_0}(\omega/T) \Theta_z(\Omega - \omega) d\omega \Big|_{\Omega=0} \quad (13)$$

The contour of integration  $C^-$  consists of a vertical path in the complex  $\omega$ -plane crossing the negative real axis at the rightmost negative real axis singularity of  $M_{v_0}(\cdot)$  and closed in an infinite semicircle in the left half plane.

Eq.(13) demonstrates that the MGF of  $v_0$ , the content of the CUT, plays an important role in

$$p_{v_0}(v) = \frac{1}{\psi} \exp\left(-\frac{v + \delta}{\psi}\right) I_0\left(2\frac{\sqrt{\delta v}}{\psi}\right) U(v) \quad (14)$$

$\delta$  denotes the signal power,  $\psi$  is the noise power,  $\delta/\psi$  represents the SNR at the square-law detector input and  $I_0(\cdot)$  stands for the modified Bessel function of type 1 and of order 0.

evaluating the probability of detection and the probability of false alarm, our strategy in analyzing a CFAR variant is to calculate its detection probability which is given by:

$$P_d = T \int_0^{\infty} p_{v_0}(Tv) F_z(v) dv \quad (10)$$

$F_z(\cdot)$  denotes the CDF of the noise power level estimate and  $T$  is a thresholding constant required to guarantee the designed rate of false alarm. In terms of the Laplace transformation, Eq.(10) takes the form:

$$P_d = T \left. \Phi_g(\Omega) \right|_{\Omega=0} \quad \text{with} \quad \Phi_g(\Omega) \triangleq \int_0^{\infty} p_{v_0}(Tv) F_z(v) \exp(-\Omega v) dv \quad (11)$$

With the aid of convolution theorem, Eq.(11) can be put in another form as:

$$\Phi_g(\Omega) = \frac{1}{T} M_{v_0}(\Omega/T) * \Theta_z(\Omega) \quad (12)$$

In the above formula,  $M_x(\cdot)$  represents the moment generating function (MGF) of the random variable (RV)  $x$ ,  $\Theta_z(\cdot)$  denotes the Laplace transformation of the CDF of the RV  $Z$ , and the symbol "\*" stands for the convolution process. By using Eq.(12), Eq.(10) can be written as:

$$P_d = \frac{1}{2\pi j} \oint_{C^-} M_{v_0}(\omega/T) \Theta_z(\Omega - \omega) d\omega \Big|_{\Omega=0} \quad (13)$$

The contour of integration  $C^-$  consists of a vertical path in the complex  $\omega$ -plane crossing the negative real axis at the rightmost negative real axis singularity of  $M_{v_0}(\cdot)$  and closed in an infinite semicircle in the left half plane.

determining the processor detection performance. Let's go to calculate this interesting parameter for the Swerling's models of fluctuating targets.

For mono-pulse application and when a non-fluctuating target return-plus-noise represents the content of the CUT, the output of this cell has a PDF given by [11]:

$$p_{v_0}(v) = \frac{1}{\psi} \left( \frac{v}{\delta} \right)^{\frac{M-1}{2}} \exp\left(-\frac{v + \delta}{\psi}\right) I_{M-1}\left(2\frac{\sqrt{\delta v}}{\psi}\right) U(v) \quad (15)$$

Since the single pulse case is infrequently used, the M-pulses form of Eq.(14) is preferable. After integrating M pulses, the new form of Eq.(14) becomes [9]:

$$p_{v_0}(v) = \frac{1}{\psi} \left( \frac{v}{\delta} \right)^{\frac{M-1}{2}} \exp\left(-\frac{v + \delta}{\psi}\right) I_{M-1}\left(2\frac{\sqrt{\delta v}}{\psi}\right) U(v) \quad (15)$$

The MGF associated with the PDF of Eq.(15) can be easily evaluated and the result yields:



$$M_{v_0}(\Omega/\delta) = \left( \frac{1}{\psi\Omega + 1} \right)^M \exp\left( -\frac{\delta\Omega}{\psi\Omega + 1} \right) \quad (16)$$

The unconditional MGF can be obtained by averaging the above formula over the target fluctuation distribution of  $\delta$ . For  $\chi^2$  family of target fluctuation models, the RV  $\delta$  is characterized by a PDF given by [18]

$$p_\delta(\delta/\bar{\delta}) = \frac{1}{\Gamma(\kappa)} \left( \frac{\kappa}{\bar{\delta}} \right)^\kappa \delta^{\kappa-1} \exp\left( -\kappa \frac{\delta}{\bar{\delta}} \right) U(\delta) \quad (17)$$

The unconditional MGF is then extracted by calculating the average value of Eq.(16) given the PDF of Eq.(17). Thus, we have

$$M_{v_0}(\Omega) = \int_0^\infty M_{v_0}(\Omega/\delta) p_\delta(\delta/\bar{\delta}) d\delta = \left( \frac{1}{\psi\Omega + 1} \right)^{M-\kappa} \left( \frac{1}{\alpha\Omega + 1} \right)^\kappa \quad \& \quad \alpha \triangleq \psi \left( 1 + \frac{\bar{\delta}/\psi}{\kappa} \right) \quad (18)$$

Eq.(18) is the fundamental formula from the Swerling's models can be derived as special cases.

#### Swerling I Model (SWI)

As Eq.(8) indicates, this model is characterized by  $\kappa=1$ . Replacing  $\kappa$  by 1 in Eq.(18) yields:

$$M_{v_0}(\Omega) = \left( \frac{1/\psi}{\Omega + 1/\psi} \right)^{M-1} \left( \frac{1/\alpha}{\Omega + 1/\alpha} \right) \quad \& \quad \alpha \triangleq \psi(1 + \bar{\delta}/\psi) = \psi(1 + \gamma) \quad (19)$$

In the above expression,  $\gamma$  denotes the average per pulse SNR. The substitution of this MGF into Eq.(13) results:

$$P_d = \frac{T}{\alpha} \left( \frac{1/\psi}{1/\psi - 1/\alpha} \right)^{M-1} \Theta_z\left( \frac{T}{\alpha} \right) + \left( \frac{T}{\psi} \right)^{M-1} \left\{ \frac{T/\alpha}{\Gamma(M-1)} \frac{d^{M-2}}{d\Omega^{M-2}} \left[ \left( \frac{1}{\Omega + T/\alpha} \right) \Theta_z(-\Omega) \right] \Big|_{\Omega=-\frac{T}{\psi}} \right\} \quad (20)$$

#### Swerling II Model (SWII)

This model of target fluctuation has an  $M^{\text{th}}$  degree of freedom. Setting  $\kappa=M$  in Eq.(18) leads to:

$$M_{v_0}(\Omega) = \left( \frac{1/\alpha}{\Omega + 1/\alpha} \right)^M \quad \& \quad \alpha \triangleq \psi \left( 1 + \frac{\bar{\delta}/\psi}{M} \right) = \psi(1 + \gamma) \quad (21)$$

$\gamma$  denotes the average, over  $M$  pulses, SNR. In this case, the processor detection performance is given by:

$$P_d = \frac{(T/\alpha)^M}{\Gamma(M)} \left. \frac{d^{M-1}}{d\Omega^{M-1}} \Theta_z(-\Omega) \right|_{\Omega=-\frac{T}{\alpha}} \quad (22)$$

#### Swerling III Model (SWIII)

This model of target fluctuation is characterized by  $\kappa=2$  in the MGF of the CUT. In this situation, the MGF of the concerned cell becomes:

$$M_{v_0}(\Omega) = \left( \frac{1/\psi}{\Omega + 1/\psi} \right)^{M-2} \left( \frac{1/\alpha}{\Omega + 1/\alpha} \right)^2 \quad \& \quad \alpha \triangleq \psi \left( 1 + \frac{\bar{\delta}/\psi}{2} \right) = \psi(1 + \gamma) \quad (23)$$

The probability of detection of SWIII target fluctuation model will be:

$$P_d = \left( \frac{T}{\alpha} \right)^2 \left( \frac{T}{\psi} \right)^{M-2} \left\{ \frac{d}{d\Omega} \left[ \left( \frac{1}{\Omega + T/\psi} \right)^{M-2} \Theta_z(-\Omega) \right] \Big|_{\Omega=-T/\alpha} + \right. \\ \left. \frac{1}{\Gamma(M-2)} \frac{d^{M-3}}{d\Omega^{M-3}} \left[ \left( \frac{1}{\Omega + T/\alpha} \right)^2 \Theta_z(-\Omega) \right] \Big|_{\Omega=-T/\psi} \right\} \quad (24)$$

*Swerling IV Model (SWIV)*

This case of target fluctuation has  $(2M)^{\text{th}}$  degrees of freedom. Thus, the substitution of  $\kappa=2M$  in Eq.(18) yields:

$$M_{\nu_0}(\Omega) = \left( \frac{1/\psi}{\Omega + 1/\psi} \right)^{-M} \left( \frac{1/\alpha}{\Omega + 1/\alpha} \right)^{2M} \quad \& \quad \alpha \triangleq \psi \left( 1 + \frac{\bar{\delta}/\psi}{2M} \right) = \psi(1 + \gamma) \quad (25)$$

Eq.(25), as a MGF, in the definition of  $P_d$  gives the processor detection performance which has a mathematical form given by:

$$P_d = \left( \frac{T}{\alpha} \right)^{2M} \left( \frac{T}{\psi} \right)^{-M} \frac{1}{\Gamma(2M)} \frac{d^{2M-1}}{d\Omega^{2M-1}} \left\{ \left( \frac{1}{\Omega + T/\psi} \right)^{-M} \Theta_z(-\Omega) \right\} \Big|_{\Omega=-T/\alpha} \quad (26)$$

In all cases, the false alarm probability takes a unified form; the mathematical version of which is:

$$P_{fa} = \left( \frac{T}{\psi} \right)^M \frac{1}{\Gamma(M)} \frac{d^{M-1}}{d\Omega^{M-1}} \left\{ \Theta_z(-\Omega) \right\} \Big|_{\Omega=-T/\psi} \quad (27)$$

Since enhancing detection performance of a CFAR variant is a basic requirement in evolving radar systems, we choose the recent version of CFAR detectors to fulfill this objective. It is intuitive that as  $P_d$  increases, the missed detection decreases and consequently, the processor performance will be enhanced. The upcoming section is devoted to evaluate the performance of the linear fusion (LF) strategy to have a knowledge about its reaction against fluctuating targets of Swerling models.

By careful examining the previous derived formulas, it is evident that they rely on the Laplace transformation of the CDF of the noise power level estimate  $Z$  and its mathematical differentiation. Therefore, we are focused on formulating this transformation when the detection scheme operates in an environment that has several outlying targets along with the main one (Tol).

### III. PROCESSOR PERFORMANCE ANALYSIS

Specifically, the efficiency of a CFAR scheme is measured in the perfect case of operating conditions or in the presence of some of fallacious targets beside the Tol. Since the ideal situation is a special case of non-ideal operation, it is preferable to analyze the processor performance in heterogeneous background. This is actually the case that we are going to follow in the upcoming subsections.

#### a) Single Adaptive Processors

##### i. Ordered-Statistics (OS)

This procedure of CFAR technology performs robustly in both inhomogeneous clutter and target multiplicity situations. It extracts the  $K^{\text{th}}$  largest sample from the candidates of the reference window to represent the estimate of the unknown noise power. To carry out such extraction, it ranks the reference cells in an ascending order, in such a way that:

$$y_{(\ell)} \leq y_{(\ell+1)} \quad \& \quad \ell = 1, 2, \dots, N-1 \quad (28)$$

In this ranked samples,  $y_{(1)}$  denotes the lowest noise level whilst  $y_{(N)}$  represents the highest one. After the rank order, we plan to pick the sample of  $K^{\text{th}}$  level to constitute the unknown noise level in the reference window. Thus, the OS test-statistic takes the form:

$$Z_{os} \triangleq y_{(K)} \quad \& \quad 1 \leq K \leq N \quad (29)$$

Aiming at evaluating the performance of the OS algorithm, this necessitates the PDF calculation of the  $K^{\text{th}}$  ordered sample in the case where the samples are independent, but not identically distributed. To accomplish such objective, let us consider that the reference window has "R" cells that contain outlying target returns each with power level  $\psi(1+\theta)$  and the

$$F_K^{NH}(t; N, R) = \sum_{i=K}^N \sum_{j=\max(0, i-R)}^{\min(i, N-R)} \binom{N-R}{j} \binom{R}{i-j} \sum_{n=0}^j \binom{j}{n} (-1)^n \sum_{m=0}^{i-j} \binom{i-j}{m} (-1)^m \{1 - F_c(t)\}^{N-R-n} \{1 - F_l(t)\}^{R-m} \quad (30)$$

In the above expression,  $F_c(\cdot)$  represents the CDF of the cell that contains clutter background whilst  $F_l(\cdot)$  denotes the same thing for the cell that has interfering target return. The random variable (RV's) representing the returns from clutter background has MGF of the same form as that given in Eq.(18) after nullifying  $\alpha$ . By using the resulting form of that equation, the Laplace transformation of  $F_c(\cdot)$  becomes:

$$\Psi_c(\Omega) = (\Omega + 1)^{-M} / \Omega \quad (31)$$

The Laplace inverse of the above formula yields:

$$F_c(t) = 1 - \sum_{\ell=0}^{M-1} \frac{t^\ell}{\Gamma(\ell+1)} e^{-t} U(t) \quad (32)$$

For the interference case, there are two situations:

a.  $\chi^2$  fluctuation with 4-degrees of freedom: if the interfering target fluctuates following this statistical type,  $F_l(\cdot)$  has a form given by [12]:

$$F_l(t) = L^{-1} \left\{ \frac{1}{\Omega} \prod_{i=1}^M \varepsilon_i^2 \frac{\Omega + 1}{(\Omega + \varepsilon_i)^2} \right\} = 1 - \sum_{\ell=1}^M (\zeta_\ell + t \xi_\ell) e^{-\varepsilon_\ell t} U(t) , \quad \varepsilon_\ell \triangleq \frac{1}{1 + 9 \lambda_\ell / 2} \quad (33)$$

Where

$$\zeta_j \triangleq \varepsilon_j (1 - \varepsilon_j)^M \prod_{\substack{i=1 \\ i \neq j}}^M \left( \frac{\varepsilon_i}{\varepsilon_i - \varepsilon_j} \right)^2 \left\{ \frac{M}{1 - \varepsilon_j} + \frac{1}{\varepsilon_j} - \sum_{\substack{\ell=1 \\ \ell \neq j}}^M \frac{2}{\varepsilon_\ell - \varepsilon_j} \right\} \quad (34)$$

and

$$\xi_j \triangleq \varepsilon_j (1 - \varepsilon_j) \prod_{\substack{k=1 \\ k \neq j}}^M \varepsilon_k^2 \frac{1 - \varepsilon_j}{(\varepsilon_k - \varepsilon_j)^2} \quad (35)$$

The substitution of Eqs.(32 & 33) into Eq.(30) leads to:

$$F_K^{NH}(t; N, R) = \sum_{i=K}^N \sum_{j=\max(0, i-R)}^{\min(i, N-R)} \binom{N-R}{j} \binom{R}{i-j} \sum_{k=0}^j \sum_{\ell=0}^{i-j} \binom{j}{k} \binom{i-j}{\ell} (-1)^{i-k-\ell} \left\{ \sum_{m=0}^{M-1} \frac{t^m}{\Gamma(m+1)} e^{-t} \right\}^{N-R-k} \left\{ \sum_{n=1}^M (\zeta_n + t \xi_n) e^{-\varepsilon_n t} \right\}^{R-\ell} \quad (36)$$

By using binomial theorem, we can expand the bracketed quantities as a binomial of t. This expansion results in reformatting Eq. (36) as:

$$\begin{aligned}
 F_K^{NH}(t; N, R) = & \sum_{i=K}^N \sum_{j=\max(0, i-R)}^{\min(i, N-R)} \binom{N-R}{j} \binom{R}{i-j} \sum_{\kappa=0}^j \sum_{\ell=0}^{i-j} \binom{j}{\kappa} \binom{i-j}{\ell} (-1)^{i-\kappa-\ell} \sum_{\alpha_0=0}^{N-R-\kappa} \sum_{\alpha_1=0}^{N-R-\kappa} \dots \sum_{\alpha_{M-1}=0}^{N-R-\kappa} \\
 & \frac{\Psi(N-R-\kappa; \alpha_0, \dots, \alpha_{M-1})}{\prod_{\nu=0}^{M-1} [\Gamma(\nu+1)]^{\alpha_\nu}} \sum_{\mu=0}^{R-\ell} \binom{R-\ell}{\mu} \sum_{\sigma_1=0}^{\mu} \sum_{\sigma_2=0}^{\mu} \dots \sum_{\sigma_M=0}^{\mu} \Psi(\mu, \sigma_1, \sigma_2, \dots, \sigma_M) \sum_{\eta_1=0}^{R-\ell-\mu} \sum_{\eta_2=0}^{R-\ell-\mu} \dots \sum_{\eta_M=0}^{R-\ell-\mu} \\
 & \Psi(R-\ell-\mu, \eta_1, \eta_2, \dots, \eta_M) \prod_{\lambda=1}^M \left( \zeta_\lambda \sigma_\lambda \xi_\lambda \eta_\lambda \right) t^{\left( R-\ell-\mu + \sum_{\beta=0}^{M-1} \beta \alpha_\beta \right)} \exp \left( - \left( N-R-\kappa + \sum_{n=1}^M (\sigma_n + \eta_n) \varepsilon_n \right) t \right)
 \end{aligned} \quad (37)$$

The Laplace transformation of Eq. (37) gives:

$$\begin{aligned}
 \Theta_K^{NH}(\Omega; N, R) = & \sum_{i=K}^N \sum_{j=\max(0, i-R)}^{\min(i, N-R)} \binom{N-R}{j} \binom{R}{i-j} \sum_{\kappa=0}^j \sum_{\ell=0}^{i-j} \binom{j}{\kappa} \binom{i-j}{\ell} (-1)^{i-\kappa-\ell} \sum_{\alpha_0=0}^{N-R-\kappa} \sum_{\alpha_1=0}^{N-R-\kappa} \dots \sum_{\alpha_{M-1}=0}^{N-R-\kappa} \\
 & \frac{\Psi(N-R-\kappa; \alpha_0, \dots, \alpha_{M-1})}{\prod_{\nu=0}^{M-1} [\Gamma(\nu+1)]^{\alpha_\nu}} \sum_{\mu=0}^{R-\ell} \binom{R-\ell}{\mu} \sum_{\sigma_1=0}^{\mu} \sum_{\sigma_2=0}^{\mu} \dots \sum_{\sigma_M=0}^{\mu} \Psi(\mu, \sigma_1, \sigma_2, \dots, \sigma_M) \sum_{\eta_1=0}^{R-\ell-\mu} \sum_{\eta_2=0}^{R-\ell-\mu} \dots \sum_{\eta_M=0}^{R-\ell-\mu} \\
 & \Psi(R-\ell-\mu, \eta_1, \eta_2, \dots, \eta_M) \prod_{\lambda=1}^M \left( \zeta_\lambda \sigma_\lambda \xi_\lambda \eta_\lambda \right) \frac{\Gamma \left( R-\ell-\mu + \sum_{\beta=0}^{M-1} \beta \alpha_\beta + 1 \right)}{\left( \Omega + N - R - \kappa + \sum_{n=1}^M (\sigma_n + \eta_n) \varepsilon_n \right)^{\left( R-\ell-\mu + \sum_{\beta=0}^{M-1} \beta \alpha_\beta + 1 \right)}}
 \end{aligned} \quad (38)$$

In the previous formulas, the term  $\Psi(J; j_1, j_2, \dots, j_M)$  is defined as [20]:s

$$\Psi(J; j_1, j_2, \dots, j_M) \triangleq \begin{cases} \frac{\Gamma(J+1)}{\prod_{i=1}^M \Gamma(j_i+1)} & \text{if } \sum_{\lambda=1}^M j_\lambda = J \\ 0 & \text{if } \sum_{\lambda=1}^M j_\lambda \neq J \end{cases} \quad (39)$$

b.  $\chi^2$  fluctuation with 2-degrees of freedom: Let us now return to the fluctuating target obeying  $\chi^2$  distribution with 2-degrees of freedom in its fluctuation. In this case,  $F_l(t)$  is given by [19]:

$$F_l(t) = L^{-1} \left\{ \frac{1}{\Omega} \prod_{\ell=1}^M \frac{\theta_\ell}{\Omega + \theta_\ell} \right\} \quad \& \quad \theta_\ell \triangleq \frac{1}{1 + \mathcal{G} \lambda_\ell} \quad (40)$$

by evaluating the Laplace inverse processing of the above formula, one obtains:

$$F_l(t) = 1 - \sum_{j=1}^M \varphi_j \exp(-\theta_j t) U(t) \quad \& \quad \varphi_j \triangleq \prod_{\substack{i=1 \\ i \neq j}}^M \frac{\theta_i}{\theta_i - \theta_j} \quad (41)$$

The substitution of Eqs.(32 & 41) into Eq.(30) yields:

$$\begin{aligned}
 F_K^{NH}(t; N, R) = & \sum_{i=K}^N \sum_{j=\max(0, i-R)}^{\min(i, N-R)} \binom{N-R}{j} \binom{R}{i-j} \sum_{\lambda=0}^j \sum_{\ell=0}^{i-j} \binom{j}{\lambda} \binom{i-j}{\ell} (-1)^{i-\lambda-\ell} \left\{ \sum_{m=0}^{M-1} \frac{t^m}{\Gamma(m+1)} e^{-t} \right\}^{N-R-\lambda} \\
 & \left\{ \sum_{n=1}^M \varphi_n e^{-\theta_n t} \right\}^{R-\ell}
 \end{aligned} \quad (42)$$

With the aid of binomial theorem, the bracketed quantities can be expanded as a binomial of  $t$ . Following this procedure of expansion, Eq.(42) can be rewritten as:

$$F_K^{NH}(t; N, R) = \sum_{i=K}^N \sum_{j=\max(0, i-R)}^{\min(i, N-R)} \binom{N-R}{j} \binom{R}{i-j} \sum_{\lambda=0}^j \binom{j}{\lambda} \sum_{\ell=0}^{i-j} \binom{i-j}{\ell} (-1)^{i-\lambda-\ell} \sum_{u_0=0}^{N-R-\lambda} \sum_{u_1=0}^{N-R-\lambda} \dots \sum_{u_{M-1}=0}^{N-R-\lambda} \frac{\Psi(N-R-\lambda; u_0, u_1, u_2, \dots, u_{M-1})}{\prod_{\sigma=0}^{M-1} [\Gamma(\sigma+1)]^{u_{\sigma}}} \sum_{v_1=0}^{R-\ell} \sum_{v_2=0}^{R-\ell} \dots \sum_{v_M=0}^{R-\ell} \Psi(R-\ell; v_1, v_2, \dots, v_M) \prod_{\eta=1}^M (\varphi_{\eta})^{v_{\eta}} t^{\sum_{\tau=0}^{M-1} u_{\tau}} \exp\left(-(N-R-\lambda + \sum_{n=1}^M v_n \theta_n) t\right) \quad (43)$$

The Laplace transformation of Eq.(43) results:

$$\Theta_K^{NH}(\Omega; N, R) = \sum_{i=K}^N \sum_{j=\max(0, i-R)}^{\min(i, N-R)} \binom{N-R}{j} \binom{R}{i-j} \sum_{\lambda=0}^j \binom{j}{\lambda} \sum_{\ell=0}^{i-j} \binom{i-j}{\ell} (-1)^{i-\lambda-\ell} \sum_{u_0=0}^{N-R-\lambda} \sum_{u_1=0}^{N-R-\lambda} \dots \sum_{u_{M-1}=0}^{N-R-\lambda} \frac{\Psi(N-R-\lambda; u_0, u_1, u_2, \dots, u_{M-1})}{\prod_{\sigma=0}^{M-1} [\Gamma(\sigma+1)]^{u_{\sigma}}} \sum_{v_1=0}^{R-\ell} \sum_{v_2=0}^{R-\ell} \dots \sum_{v_M=0}^{R-\ell} \Psi(R-\ell; v_1, v_2, \dots, v_M) \prod_{\eta=1}^M (\varphi_{\eta})^{v_{\eta}} \frac{\Gamma\left(\sum_{\tau=0}^{M-1} u_{\tau} + 1\right)}{\left(\Omega + N - R - \lambda + \sum_{n=1}^M v_n \theta_n\right)^{\left(\sum_{\tau=0}^{M-1} u_{\tau} + 1\right)}} \quad (44)$$

Once Eqs. (38 & 44) are obtained, the false alarm and detection performances are completely evaluated, as Eqs.(20, 22, 24, 26, 27) demonstrate. The major drawback of this scheme is the high processing time that is taken in performing the sorting mechanism.

## ii. Trimmed-Mean (TM)

The trimmed-mean (TM) algorithm is the more generalized version of the OS scheme. It may be considered as an amended version of the OS scenario. The motivation of using this algorithm is to combine the benefits of averaging and ordering along with censoring. In this scheme, the noise power is estimated by a linear combination of some selected ordered range samples.

$$Z_{TM}(L_1, L_2) \triangleq$$

Clearly, the ordered samples  $y_{(i)}$ 's are neither independent nor identically distributed, so the performance evaluation of TM scheme becomes cumbersome. To handle this evaluation, a new linear

linear combination may be anticipated to give better results because averaging estimates the noise power more efficiently as in the case of the CA processor and thus loss of detection in uniform background is more tolerable. In the TM-CFAR detector, the lowest  $L_1$  ordered range samples and the highest  $L_2$  ordered ones are excised before summing the remaining cells to formulate the statistic  $Z_{TM}$ . Thus,

$$\sum_{\ell=L_1+1}^{N-L_2} y_{(\ell)} \quad (45)$$

transformation is needed. In other words, the following transformation can be used to make the ordered samples  $y_{(i)}$ 's satisfy the IID property [18]. Mathematically, this transformation takes the form:

$$Y_{\ell} \triangleq y_{(L_1+\ell)} - y_{(L_1+L_2)} U(\ell-2) \quad (46)$$

As a function of these new variables  $Y_i$ 's, Eq.(45) can be rewritten as:

$$Z_{TM}(L_1, L_2) = \sum_{j=1}^{L_T} (L_T - j + 1) Y_j \quad \& \quad L_T \triangleq N - L_1 - L_2 \quad (47)$$

In terms of the  $\Omega$ -domain representation of the CDF of the ordered samples  $y_{(i)}$ 's, the MGF of the random variables  $Y_j$ 's can be easily calculated as [12]:

$$M_{Y_j}(\Omega) = \begin{cases} \Omega \Theta_{L_1+1}^{NH}(\Omega; N, R) & \text{for } j = 1 \\ \frac{\Theta_{L_1+j}^{NH}(\Omega; N, R)}{\Theta_{L_1+j-1}^{NH}(\Omega; N, R)} & \text{for } 1 < j \leq L_T \end{cases} \quad (48)$$

After obtaining the formula (48), the computation of the MGF of the noise level estimate  $Z_{TM}$  becomes an easy task owing to the independency of its samples. Thus,

$$M_{Z_{TM}}(\Omega; L_1, L_2) = \prod_{\ell=1}^{L_T} M_{Y_\ell}(\Omega) \Big|_{\Omega = (L_T - \ell + 1)\Omega} \quad (49)$$

Though the TM-CFAR scheme offers good performance, the large processing time, which is taken in ordering the candidates of the reference window, limits its practical applications. This problem can be overcome by partitioning the reference window into Q, symmetrical or nonsymmetrical, smaller sub-windows. The samples in the each sub-window are processed and its statistic  $Z$  may be estimated according to a specified rule and the final statistic is chosen by further processing the Q sub-window outputs. Here, we apply this idea by symmetrically partitioned the reference window into preceding and succeeding sub-windows ( $Q=2$ ). In this situation, suppose that the preceding subset has  $R_1$  cells from outlying target returns,  $N/2-R_1$  ones from thermal background, the lowest  $P_1$  cells and the highest  $P_2$  ones are censored from its ordered-statistic before adding the remaining cells to establish

$$Z_f = \text{Mean}(Z_1, Z_2) \quad (50)$$

Since the two noise level estimates are statistically independent, the final noise level estimate has a MGF given by:

$$M_{Z_f}(\Omega) = M_{Z_{TM}}(\Omega; P_1, P_2) M_{Z_{TM}}(\Omega; S_1, S_2) \quad (51)$$

As Eqs.(20, 22, 24, 26, 27) indicate that the probabilities of detection and false alarm are functions of the Laplace transformation of the CDF of the noise

the background level of the preceding sub-window. Similarly, assume that the succeeding sub-window has  $R_2$  cells of fallacious target returns,  $N/2-R_2$  samples containing clutter, its associated ordered-statistic is trimmed from its ends, where the lowest  $S_1$  ordered cells are excised and  $S_2$  highest ranked cells are nullified. Under these circumstances, the MGF's of their noise power level estimates,  $Z_1$  and  $Z_2$ , have the same form as that given by Eq.(49) after replacing its common parameters with their corresponding values for the preceding and succeeding subsets. Since the mean-level (ML) operation represents the simplest way that uses arithmetic averaging to extract the unknown noise power level, the two noise level estimates are combined through the ML operation to formulate the final noise power estimate. Mathematically, this can be expressed as:

level estimate  $Z_f$ , it is necessary to compute such important parameter. As a function of the MGF of  $Z_f$ , its CDF has a Laplace transformation given by [21]:

$$\Theta_{Z_f}(\Omega) = M_{Z_f}(\Omega) / \Omega \quad (52)$$

Once the  $\Omega$ -domain representation of the PDF of the resultant noise level estimate is formulated, the processor false alarm and detection performances can be completely evaluated, as we have proved in the previous section. It is of importance to note that the TM scenario reduces to the conventional CA and OS

algorithms for specific trimming values. In other words, TM (0, 0) and TM (K-1, N-K) tend to the well-known CA and OS (K) processors, respectively; each handles N reference cells to estimate the unknown noise power level. Thus, for the conventional CA and OS (K) schemes, we have:

and

$$M_{Z_{CA}}(\Omega) = M_{Z_{TM}}(\Omega;0,0)M_{Z_{TM}}(\Omega;0,0) \quad (53)$$

In Eq.(53), the noise levels extracted from the preceding and succeeding sub-windows of the OS scheme are:

$$Z_1 \triangleq y_{(K_1)} \quad \& \quad Z_2 \triangleq y_{(K_2)} , \quad K_1, K_2 \in \left(1, 2, \dots, \frac{N}{2}\right) \quad (55)$$

### iii. Cell-Averaging (CA)

The CA is the king of the CFAR schemes that has the highest homogeneous performance, given that the clutter is exponentially distributed and the contents of the reference window are IID. It uses the maximum likelihood estimate of the noise power to set the adaptive threshold. The CA performs the traditional averaging technique by dividing the summing of the contents of the reference cells by their number. Commonly, it is regarded as the reference model against which new implementations are compared. Nevertheless, it exhibits a weak behavior against heterogeneous background which are frequently created by clutter edges and the appearance of multiple target situations. If one or more spurious targets fall within the reference window, the probability of losing the targets will be increased owing to the severe phenomenon of target masking.

Since CA is a special case of TM scheme, we can exploit the analysis of the TM variant to evaluate the performance of the CA detector, where all of its ordered samples are activated. Thus, under the same conditions of the double-window TM scenario, the MGF of the double-window CA processor is given by Eq.(53).

#### b) Combined CFAR Schemes

##### i. Linear Fusion (LF) Emerged Strategy

A robust detector should not only pick out targets but also diminish false alarms. For target detection in complex background, it is difficult to realize high level of detection simultaneously with holding low rate of false alarm. Therefore, an effective detector dictates an incorporation of different features in such a way that each aspect resolves one of the challenges that enface the detection characteristics. In other words, an architecture involving decentralized processing at multiple sensor locations provides the proper choice of optimum results in heterogeneous situation. From this point of view, the fusion strategy has rapidly become a methodology of choice for detecting fluctuating targets. Such establishment involves higher reliability and survivability, along with improved system performance at low latency. In this scenario of CFAR technology, a

Fig.(1) portrays the detailed architecture of such developed model. In this layout, there are three individual arms in accordance with the standard detectors. Depending on the required rate of false alarm, the detection threshold along with the signal strength of the CUT of each local scheme is used to reach the final decision about the presence/absence of the target under research. According to the appropriate fusion rule, the three local decisions are simultaneously mixed in the fusion center to establish the final decision. As the circuit of Fig.(1) depicts, the potential outputs of fusion CA\_OS\_TM strategy are summarized in Table I. Since the CA scheme provides a low false alarm rate and a high level of detection, its output is taken as a baseline for the fusion center. When the CA output is positive (presence of target), there is a possibility of occurrence of false alarm, caused by clutter transition or target multiplicity. To eliminate this eventuality, the AND fusion Rule(I), indicated in Eq.(56), can be applied. This rule necessitates the application of an AND logic between the CA output and that obtained by applying an OR logic between the outputs of OS and TM schemes. On the other hand, when the CA output is negative (absence of target), there exists the possibility of a target lost caused by clutter interference. To avoid such occurrence, an AND fusion Rule(II), exhibited in Eq.(56) is utilized. This involves the application of an AND logic between the outputs of OS and TM variants.

$$Rule = \begin{cases} I & CA \wedge (OS \vee TM) \\ II & OS \wedge TM \end{cases} \quad (56)$$

In the previous expression, "v" stands for the algebraic Boolean of OR gate whilst " $\wedge$ " represents the same thing of AND gate.

Table 1: Possible Outcomes of Linear Fusion Strategy

CA Scenario	OS Procedure	TM Strategy	FUSION RULE
Absence	Absence	Absence	Absence
Absence	Absence	Presence	Absence
Absence	Presence	Absence	Absence
Absence	Presence	Presence	Presence
Presence	Absence	Absence	Absence
Presence	Absence	Presence	Presence
Presence	Presence	Absence	Presence
Presence	Presence	Presence	Presence

As Table I indicates, the appearance of Tol is demonstrated by the outcomes of rows 4, 6, 7, and 8. Since the occurrence of one of them excludes the occurrence of the others, they are mutually exclusive. Taking into account that the decisions of CA, OS, and

TM approaches are independent events, the global detection probability " $P_{LF}$ " of the new implementation can be obtained by summing the outcomes of these rows. Thus,  $P_{LF}$  has a mathematical form given by:

$$\begin{aligned} P_{LF} &= P_{miss_{CA}} P_{d_{OS}} P_{d_{TM}} + P_{d_{CA}} P_{miss_{OS}} P_{d_{TM}} + P_{d_{CA}} P_{d_{OS}} P_{miss_{TM}} + P_{d_{CA}} P_{d_{OS}} P_{d_{TM}} \\ &= P_{d_{CA}} (P_{d_{OS}} - 2 P_{d_{OS}} P_{d_{TM}} + P_{d_{TM}}) + P_{d_{OS}} P_{d_{TM}} \end{aligned} \quad (57)$$

Here,  $P_{miss}$  denotes the probability of missed detection. All the parameters of Eq.(57) are previously calculated. So, the detection performance of the LF-CFAR strategy is completely analyzed.

Our scope in the upcoming section is to numerically simulate the derived formulas through a PC device using C++ programming language to see the new contribution of the LF style in the CFAR world.

#### IV. SIMULATION RESULTS AND DISCUSSION

It is of importance to numerically evaluate the performance of the examined model. This section introduces the simulation results in order to confirm the performance superiority of the proposed algorithm. How well the model reacts against the presence of inhomogeneous background, can be assessed by several parameters. The most dominant and common ones include detection performance, CFAR loss, and actual probability of false alarm which measures the model's capability of holding the rate of false alarm stationary en face of outliers. Thus, we go to compute the detection performance, in the absence as well as in the presence of fallacious targets, for two and four ( $M=2$  & 4) post-detection integrated pulses to see to what extent the pulse integration can ameliorate the reaction of the CFAR scheme against fluctuating targets. In our simulated results, it is assumed that the reference window has a size ( $N$ ) of 24 cells, the designed  $P_{fa}$  is  $10^{-6}$ . For OS scenario, the 10<sup>th</sup> ordered sample, OS(10),

is chosen to represent its noise level estimate of each reference sub-window, whilst for TM scheme, the two smallest cells along with the two highest ones, TM(2, 2), are excised from the ordered set of each sub-window before adding the remaining ordered samples to extract its background power. Since the double-windows and mean-level operation are common for all the CFAR processors under test, it is of preferable to omit these features from nominating them. Instead, it is sufficient to designate each one of them with the CFAR rule used in estimating the unknown noise level of each sub-window as CA, OS(10) and TM(2, 2).

Fig.(2) shows the level of detection as a function of primary target signal strength (SNR) of the new methodology in homogeneous environment for the four Swerling models when the CFAR circuit based its decision on integrating two ( $M=2$ ) consecutive sweeps. For the sake of comparison, the single sweep ( $M=1$ ) case is attached for  $\chi^2$  fluctuating target with two ( $\kappa=1$ ) and four ( $\kappa=2$ ) degrees of freedom. Additionally, the same results of the optimum (N-P) detector are included among the curves of Fig.(2). In the case of single pulse operation, the displayed results illustrate that there is a turnover point; below which the N-P scheme surpasses, in detection performance, the LF strategy whilst upper this point the reverse is occurred. In other words, when the target signal is strengthened, the detection performance of the new variant outweighs that of the N-P detector and the gap between the two curves



increases as the signal becomes more strengthened. Moreover, the processor performance for fluctuating targets with  $\kappa=2$  is higher than that obtained for  $\kappa=1$  and this behavior is noticed for LF and N-P processors given that the turnover point is exceeded. Furthermore, the performance of SWI model coincides with that of SWII model and the performances of SWIII and SWIV models are the same.

For  $M=2$ , on the other hand, it is noted that the turnover point is shifted towards lower signal strength. At the preceding of this point, SWI has the top performance whereas SWIV gives the worst detection level. As this point is surpassed, the reverse is observed; where SWIV model has the highest performance whilst the SWI model exhibits the lowest probability of detection. It is of importance to note that the detector performance against SWII fluctuation model coincides with that corresponds to SWIII model in the case where the radar receiver has a non-coherent integration of two successive pulses ( $M=2$ ) as Eq.(8) demonstrates. As we have noticed for  $M=1$ , the N-P detector has a detection performance which is meagerly superior, at lower SNR, than that of LF scheme, when the turnover point is not reached. When the SNR is greater than that corresponding to the turnover point, the new methodology has the top performance whatever the fluctuation model is. The gap between the two curves (LF & N-P) corresponding to SWI model is the widest whereas this gap is narrow for SWIV model, taking into account that the LF strategy has always the top performance against any fluctuation model.

Fig.(3) illustrates the same thing as that presented in Fig.(2) on the exception that the operating environment is contaminated with some interfering targets instead of being free of them. The results of this scene are obtained on the assumption that one of each reference sub-window cells contains interfering target return ( $R_1=R_2=1$ ); the signal strength of which equals to that of the primary target ( $\text{INR}=\text{SNR}$ ) and follows the same Swerling model, as the target of interest, in its fluctuation. A big insight on the variation of the curves of this plot indicates that the turnover points of LF and N-P are different, instead of coincide as in homogeneous case in Fig.(2), and this occurs either the pulse integration is absent ( $M=1$ ) or present ( $M=2$ ). In addition, the N-P detector has the top performance especially when the signal strength is modest. As the target echo becomes strengthened, the detection performance of the new processor approaches that of the N-P and may surpass it if the CFAR circuit is provided by pulse integration, as Fig.(3) demonstrates. Moreover, the point of exceeding for SWI fluctuation model takes place at a SNR which is lower than that occurs for SWII model which in turn precedes, in its location, that associated with SWIV model. It is of importance to note that this behavior doesn't appear if

pulse integration doesn't achieve. The single sweep performance confirms this knowledge.

Fig.(4) repeats the behavior of LF and N-P, against fluctuating targets, when the operating environment is ideal (homogeneous) as that displayed in Fig.(2) with the exception that the radar receiver builds its decision on integrating four ( $M=4$ ), instead of two ( $M=2$ ), successive pulses. The portrayed results of this figure prove that the candidates of this figure have the same variation as those corresponding in Fig.(2) within some gain. Additionally, the gap between the performance of novel scheme and that of N-P becomes evident; with LF detector always on the top given that the signal strength exceeds the turnover point.

Similarly, Fig.(5) redraws the results of Fig.(3) for  $M=4$  under the same circumstances. In comparison with the results of Fig.(3), the current results exhibit some noticeable remarks as: the gap between the LF performance and optimum (N-P) is narrower, the point of exceeding is shifted towards lower SNR with the same sequence of Swerling models as that outlined during our comments on the curves of Fig.(3), and there is an evident gain in the performance of the examined and standard detectors.

Now, Let us go to evaluate another figure of merit which is known as CFAR loss. Fig.(6) shows how the signal strength must be to satisfy a detection level of 90% ( $P_d=0.9$ ) as a function of the correlation strength among the primary target returns when this target obeys  $\chi^2$ -statistics, with two ( $\kappa=1$ ) degrees of freedom, in its fluctuation. As a reference of comparison, the traditional CFAR and N-P schemes are incorporated among the results of the LF style. The displayed results are acquired on the assumption that the environment of operation is ideal and two ( $M=2$ ) consecutive sweeps are non-coherently integrated. A big insight on the behavior of the curves of this figure demonstrates that as the correlation among the target returns increases, the echo signal must be more strengthened to reply the required level of detection. Additionally, the conventional OS scenario needs the highest, relative to the other ones stated here, signal power to attain 90% level of detection, the standard TM mechanism comes next, the traditional CA procedure reserves the third position, the optimum (N-P) occupies the fourth location, whilst the new methodology (LF) needs the minimum signal strength in order to accomplish the requested probability of detection. The results of this scene reveals the superiority of the underlined detector over its original ones as well as the N-P which is taken as a reference of any new variant added to the CFAR world. Fig.(7) depicts the same behavior for the concerned processors when the primary target fluctuates in accordance with  $\chi^2$ -statistics, with four ( $\kappa=2$ ) degrees of freedom. The tested variants follow the same sequence, as indicated in Fig.(6), in demanding the signal strength to reply a detection level of 90%. Moreover, for any one

of the examined schemes, the signal power required in this situation is weaker than that needed in Fig.(6) to satisfy the same probability of detection.

In multiple target situations, Figs.(8-11) illustrate the needed signal strength to satisfy a given level of detection when the primary and the secondary targets follow SWI, SWII, SWIII, and SWIV models, respectively, in their fluctuation for the underlined detectors given that the decision is carried out based on integrating two ( $M=2$ ) successive pulses and the outlying target returns have the same signal strength as those of primary target ( $\vartheta=\gamma$ ).

As a reference of comparison, the results of the N-P scheme are included among the curves of these figures under the same target fluctuation model. Fig.(8) portrays the required signal power versus the pre-assigned level of detection for the standard as well as the derived versions when one cell among the contents of each reference sub-window is contaminated with extraneous target returns ( $R_1=R_2=1$ ). The displayed results illustrate that the CA technique can reply the request probability of detection till a specified level beyond which it hasn't the capability to satisfy the needed level of detection whatever the signal strength is. In this regard, we define the dynamic range as the range belong to which, the CFAR processor can reply any given level of detection. Based on this definition, the CA scheme has a limited dynamic range which is very narrow. All the other under-examination processors are able to reply any level of detection with different signal powers. For lower values of detection probability, there is a gap between the signal strengths needed by LF strategy and N-P detector with LF needs the highest. However, as the pre-assigned detection level increases, this gap becomes narrower till the two curves coincide and may LF requests the lowest signal strength to verify the high levels of detection. The OS(10), TM(2, 2), and LF scenarios have full dynamic range, with OS(10) demands the highest whilst LF needs the lowest signal power to give the pre-assigned level of detection. In addition, the length of the dynamic range of CA detector varies as a function of the target fluctuation model in such a way that SWI model gives smallest whilst SWIV model results in relatively the largest extend of the dynamic range. The remaining schemes have always the full length for their dynamic range irrespective the fluctuation model is. However, the required signal strength varies depending on the model of fluctuation in such a way that the SWI model requires the highest whereas the SWIV model needs the lowest signal power to reply the same level of detection.

Finally, we are going to test the capability of the new methodology of holding the rate of false alarm unchanged en face of fallacious target returns that may exist among the contents of the reference sub-windows. This category of plots includes Figs.(12 & 13). While Fig.(12) is devoted to measure the actual false alarm

rate, as a function of the correlation strength among the interferer's returns, in the case where the outliers fluctuate following  $\chi^2$ -distribution with two-degrees ( $\kappa=1$ ) of freedom, Fig.(13) depicts the same thing for  $\chi^2$ -distribution with four-degrees ( $\kappa=2$ ) of freedom for the fluctuation of the interferers. In these two figures, it is assumed that each reference sub-window has only one contaminated cell ( $R_1=R_2=1$ ) and the interference strength has a power of 10dB ( $\vartheta=10$ dB). In addition, the data of these figures is established taking into account that the CFAR circuit non-coherently integrates two successive pulses ( $M=2$ ). The displayed results of Figs.(12 & 13) demonstrate that the LF derived version has the ability of maintaining the false alarm rate, as the standard OS(10) and TM(2, 2) procedures, whatever the strength of correlation among interferer's returns is. As predicted, the conventional CA detector is incapable of fixing the rate of false alarm against the existence of outlier's returns.

## V. CONCLUSIONS

According to the analysis outlined above, the current investigation is aimed at comparing the performance of several CFAR alternatives regarding the maintaining of the false alarm probability and the reaching of the top of detection probability with the goal of selecting the most promising CFARs. For the Swerling target models, embedded in white Gaussian noise of unknown level, we derive an analytical expression for the overall probability of detection while the overall probability of false alarm is retained at the desired level for the given fusion rules. Through extensive simulations, the superiority and robustness of the linear fusion mechanism are clearly demonstrated by outperforming the conventional processors of CA, OS, TM and N-P in scenarios with different target fluctuation models, different correlation strengths among the target's returns, different numbers of integrated pulses, and varied operating circumstances. This ability to obtain improved performance compared to existing models is the major contribution of this work. In other words, performance analysis, conducted on both analytical and simulated results, highlights that the new architecture operating in multi-target background guarantees the constant false alarm rate property with respect to the correlation strength variations and a limited detection loss with respect to the other detectors, whose detection thresholds nevertheless are very sensitive to the interference power. The cost is that LF-CFAR suffers from more computational burden and elapsed time than other processors. We conclude from our simulation results that the fusion detector has higher quality detection interactions in heterogeneous environments. In other words, the linear fusion enjoy significant advantages in both the false alarm regulation property and detection performance, as the displayed results of



this research demonstrated. Thus, the LF strategy has the proficiency of choice en face of heterogeneous situations.

## REFERENCES RÉFÉRENCES REFERENCIAS

1. W. Q. Wang, "Radar Systems: Technology, Principles and Applications", Nova Science Publishers, Inc, 2013.
2. El Mashade, M. B., "Monopulse detection analysis of the trimmed mean CFAR processor in nonhomogeneous situations", IEE Proc. Radar, Sonar Navig., Vol. 143, No. 2 , pp.87-94, April 1996.
3. El Mashade, M. B., "Partially correlated sweeps detection analysis of mean-level detector with and without censoring in non ideal background conditions", Int. J. Electron. Commun. (AEÚ), Vol.53, No.1, (Feb. 1999), pp. 33-44.
4. A. Farrouki and M. Barkat, "Automatic censoring CFAR detector based on ordered data variability for nonhomogeneous environments", IEE Proc.-Radar Sonar Navig., Vol. 152, No. 1, pp.43-51, February 2005.
5. El Mashade, M. B., "Analysis of Cell-Averaging Based Detectors for  $\chi^2$  Fluctuating Targets in Multitarget Environments", Journal of Electronics (China), Vol.23, No.6, (November 2006), pp. 853-863.
6. L. Zhao, W. Liu, X. Wu and J.S. Fu, "A novel approach for CFAR processors design", Proc. of the IEEE International Conference on Radar, Atlanta, GA, 1-3 May 2001, pp. 284-288.
7. Santos Lopez-Estrada, René Cumplido, "Fusion center with neural network for target detection in background clutter", Proc. of the Sixth Mexican International Conference on Computer Science (ENC'05), 2005.
8. Toufik Laroussi, Mourad Barkat and Nassim Benadjina, "A Performance Comparison of two time Diversity Systems using TM-CFAR Detection for Partially Correlated Chi-Square Targets in Nonuniform Clutter and Multiple Target Situations", 2007 IEEE International Conference on Signal Processing and Communications (ICSPC 2007), 24-27 November 2007, Dubai, United Arab Emirates.
9. El Mashade, M. B., "Analytical Performance Evaluation of Optimum Detection of  $\chi^2$  Fluctuating Targets with M-Integrated Pulses", Electrical and Electronic Engineering, Vol. 1, No. 2, pp. 93-111, 2011.
10. Anatolii A. Kononov, Jin-Ha Kim, Jin-Ki Kim, and Gyoungju Kim, "A New Class of Adaptive CFAR Methods for Nonhomogeneous Environments", Progress In Electromagnetics Research B, Vol. 64, 145-170, 2015.
11. Md. Maynul Islam, Mohammed Hossam-E-Haider, "Detection Capability and CFAR Loss Under Fluctuating Targets of Different Swerling Model for Various Gamma Parameters in radar", (IJACSA) International Journal of Advanced Computer Science and Applications, Vol. 9, No. 2, pp.90-93, 2018
12. El Mashade, M. B., "Performance superiority of CA\_TM model over N-P algorithm in detecting  $\chi^2$  fluctuating targets with four-degrees of freedom", Int. J. Systems, Control and Communications, Vol. 11, No. 1, pp. 92-118, 2020.
13. D. Ivković, B. Zrnić and M. Andrić, "Fusion CFAR detector in receiver of the software defined radar", Proc. of the International Radar Symposium IRS-2013, Dresden, Germany, 19-21 June 2013.
14. El Mashade, M. B., "Performance Analysis of OS Structure of CFAR Detectors in Fluctuating Target Environments", Progress In Electromagnetics Research C, Vol.2, pp. 127-158, 2008.
15. El Mashade, M. B., "Partially-Correlated  $\chi^2$  Targets Detection Analysis of GTM-Adaptive Processor in the Presence of Outliers", I.J. Image, Graphics and Signal Processing, Vol. 7, No. 12, pp. 70-90, Dec. 2014.
16. El Mashade, M. B., "Adaptive Detection Enhancement of Partially-Correlated  $\chi^2$  Targets in an Environment of Saturated Interference", Recent Advances in Electrical & Electronic Engineering, Vol. 9, No. 2, pp.1-21, 2016.
17. J. R. Machado-Fernández, N. Mojena-Hernández, J. Bacallao-Vidal, "Evaluation of CFAR detectors performance", ITECKNE Vol. 14, No. 2, December 2017, pp.170 – 178.
18. El Mashade, M. B., "Heterogeneous Performance Analysis of the New Model of CFAR Detectors for Partially-Correlated  $\chi^2$ -Targets", Journal of Systems Engineering and Electronics, Vol. 29, No. 1, February 2018, pp.1 – 9.
19. El Mashade, M. B., "M-Sweeps multi-target analysis of new category of adaptive schemes for detecting  $\chi^2$ -fluctuating targets", Journal of Information and Telecommunication, Vol. 4, No. 3, 314–345, 2020.
20. El Mashade, M. B., "Inhomogeneous Performance Evaluation of a New Methodology for Fluctuating Target Adaptive Detection", Progress In Electromagnetics Research C, Vol. 107, 273–286, 2021.
21. El Mashade, M. B., "Inhomogeneous Analysis of Novel Model of CFAR Approaches to Detect Two-Degrees of Freedom Partially-Correlated  $\chi^2$ -Targets", WSEAS Transactions on Communications, Vol. 20, pp.28-43, 2021.

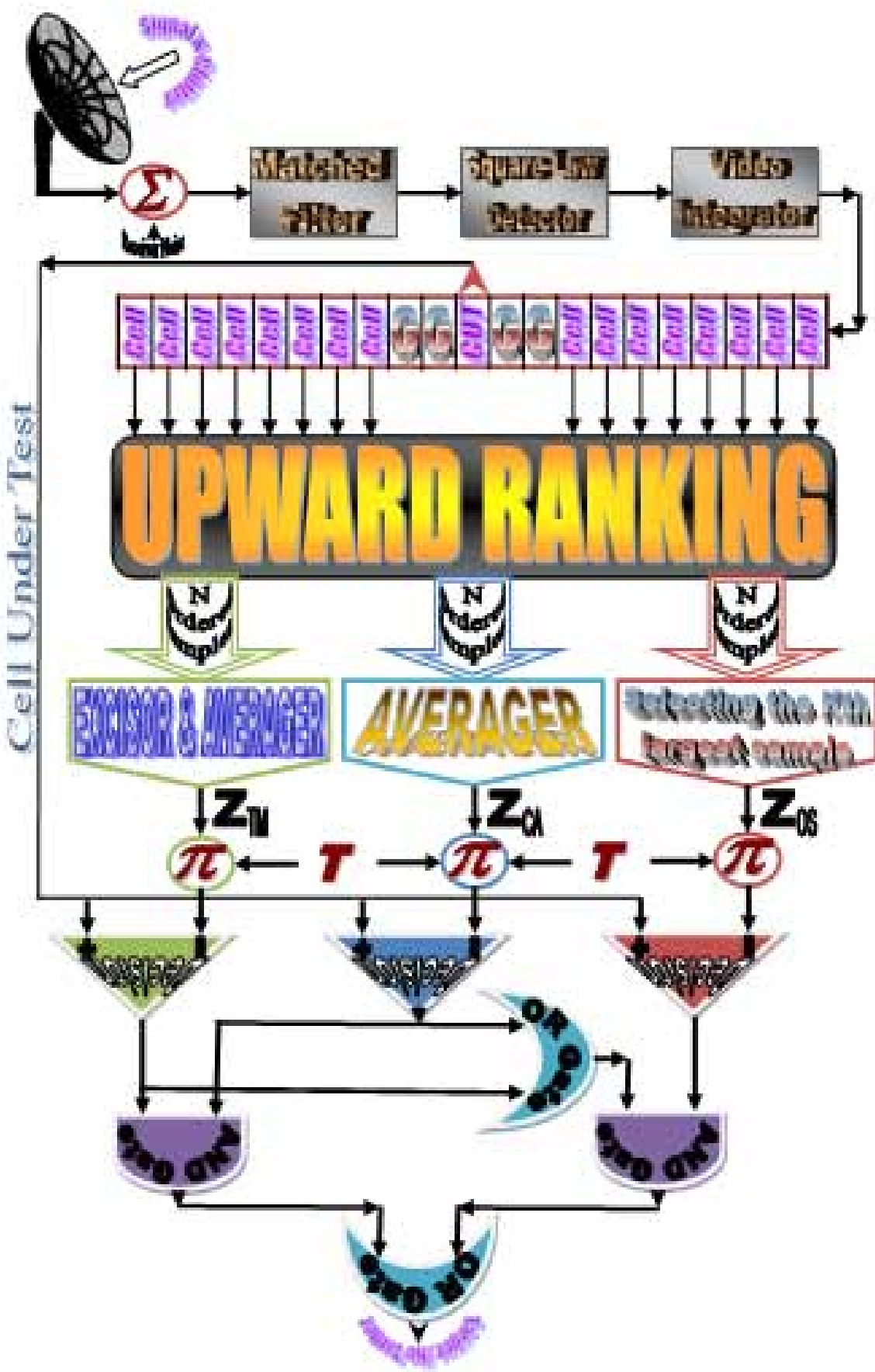


Fig. (1): Architecture of linear fusion (LF) adaptive detector with postdetection integration

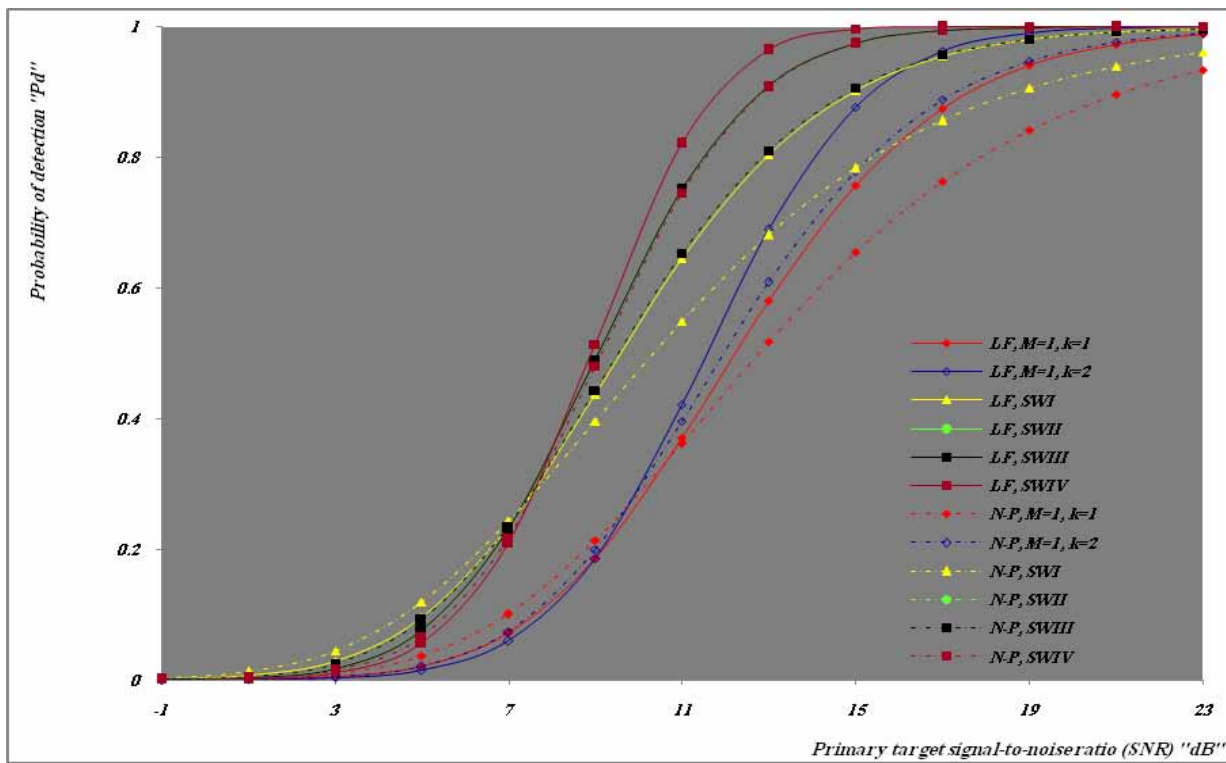


Fig. (2): M-sweeps homogeneous detection performance of LF and N-P schemes for Swerling models of  $\chi^2$ -fluctuating targets when  $N=24$ ,  $M=2$ , and  $P_{fa}=10^{-6}$

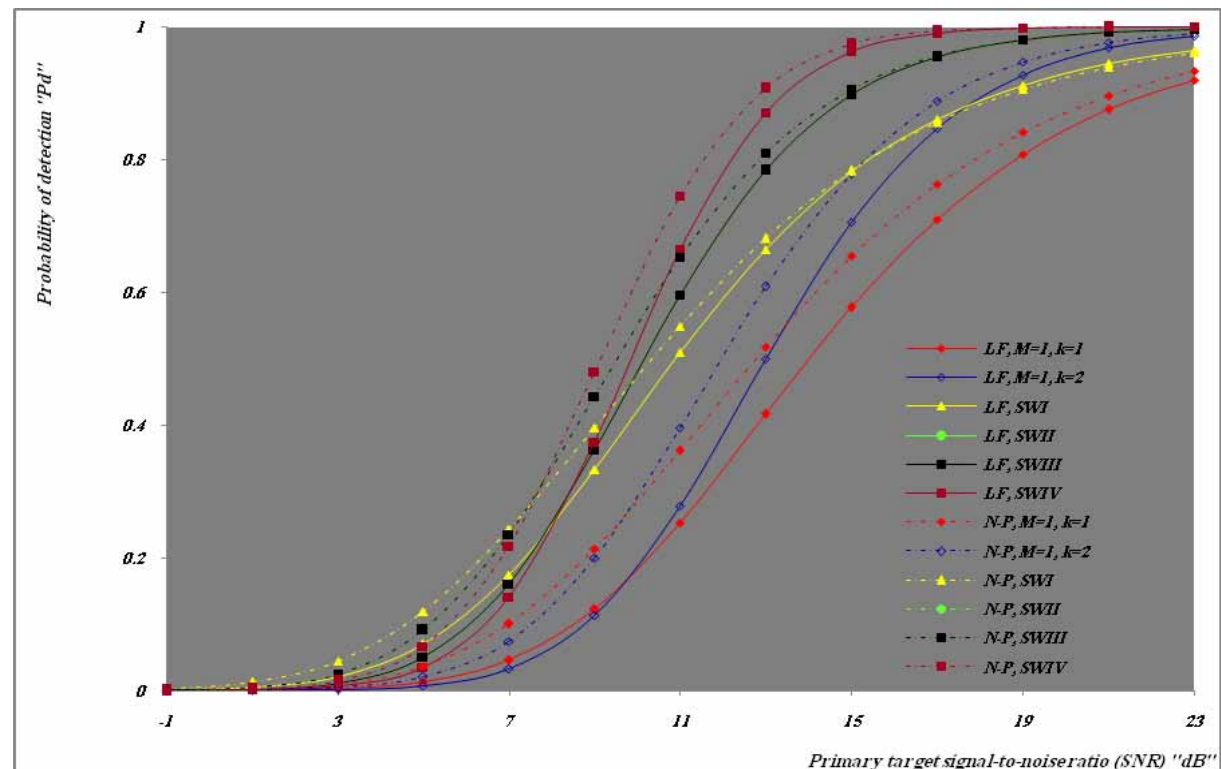


Fig. (3): M-sweeps multi-target detection performance of LF and N-P schemes for Swerling models of  $\chi^2$ -fluctuating targets when  $N=24$ ,  $M=2$ ,  $R_1=R_2=1$ ,  $\theta=\gamma$ ,  $\rho_s=\rho_p$ , and  $P_{fa}=10^{-6}$

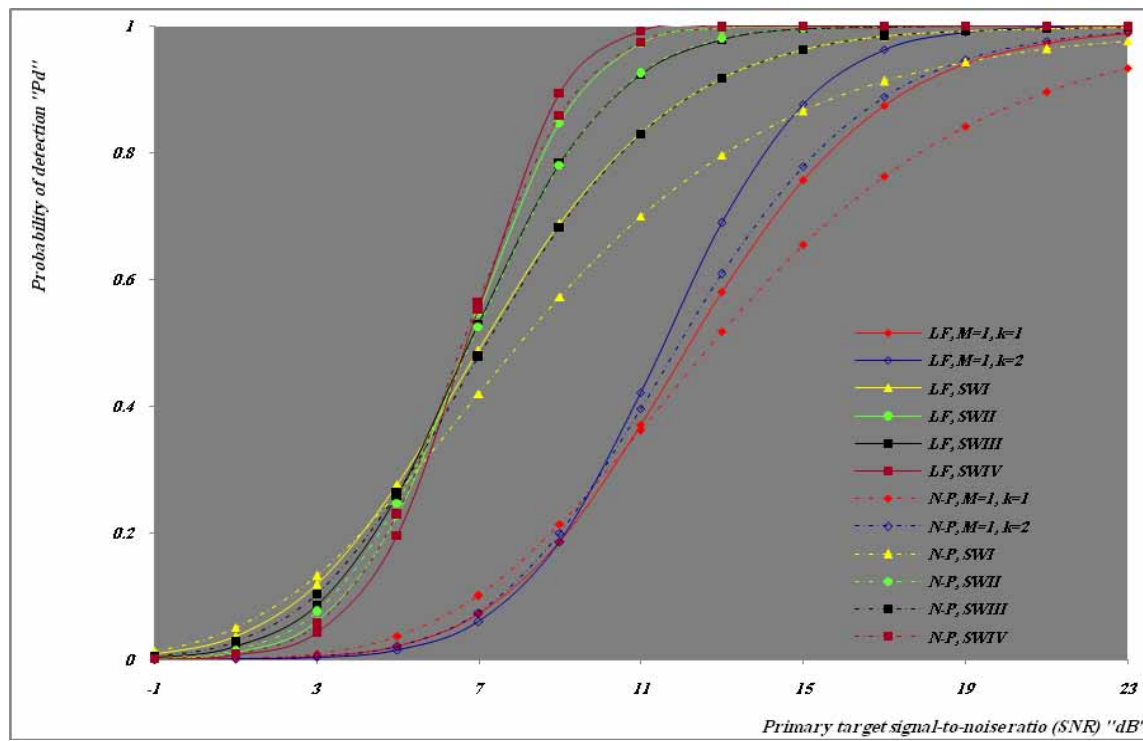


Fig. (4): M-sweeps homogeneous detection performance of LF and N-P schemes for Swerling models of  $\chi^2$ -fluctuating targets when  $N=24$ ,  $M=4$ , and  $P_{fa}=10^{-6}$

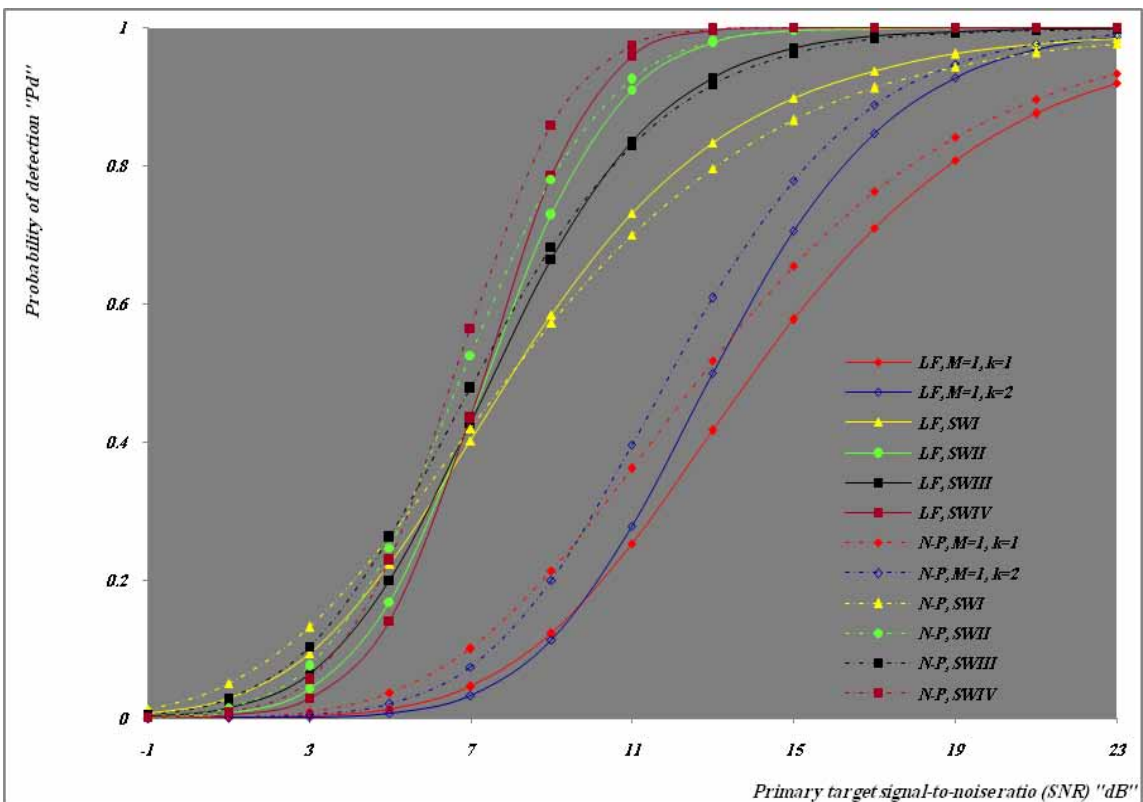


Fig. (5): M-sweeps multi-target detection performance of LF and N-P schemes for Swerling models of  $\chi^2$ -fluctuating targets when  $N=24$ ,  $M=4$ ,  $R_1=R_2=1$ ,  $\theta=\gamma$ ,  $\rho_s=\rho_p$ , and  $P_{fa}=10^{-6}$

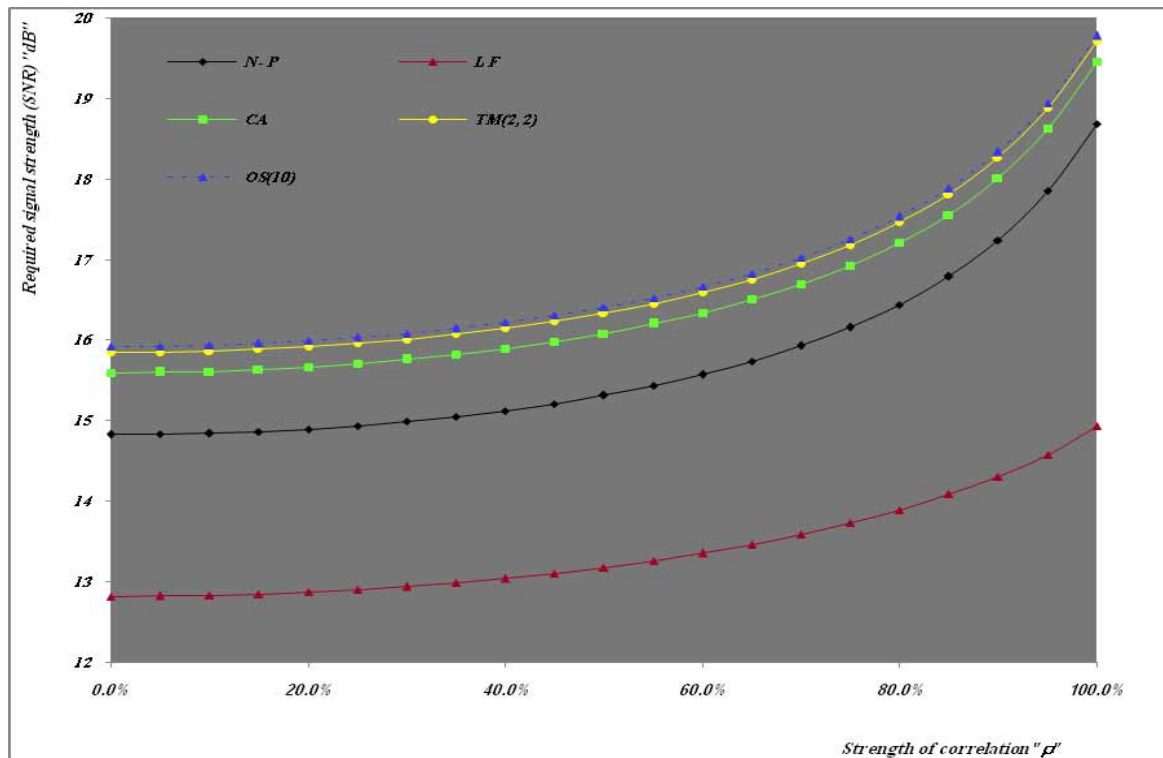


Fig. (6): M-sweeps homogeneous signal strength requested to achieve a detection level of 90% of CFAR schemes for second-degree of freedom  $\chi^2$ -fluctuating targets when  $N=24$ ,  $M=2$ , and  $P_{fa}=10^{-6}$

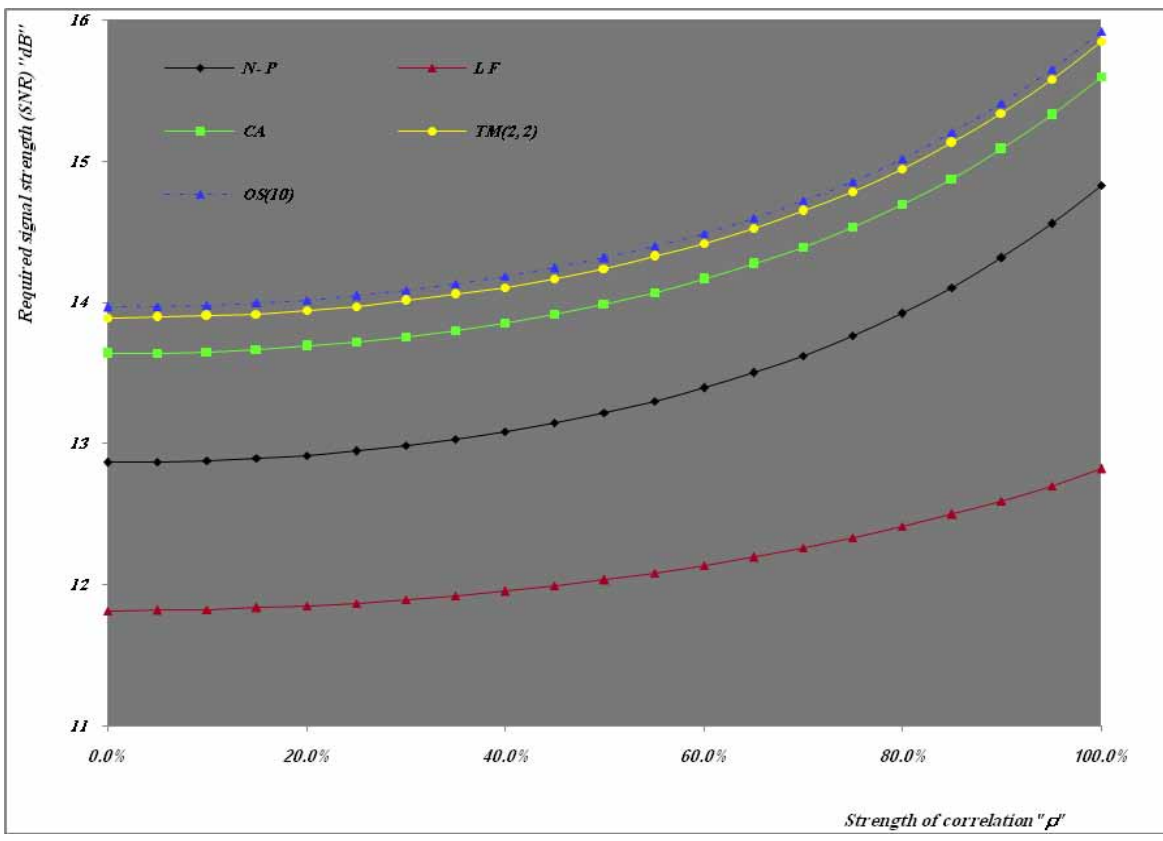


Fig. (7): M-sweeps homogeneous signal strength requested to achieve a detection level of 90% of CFAR schemes for fourth-degree of freedom  $\chi^2$ -fluctuating targets when  $N=24$ ,  $M=2$ , and  $P_{fa}=10^{-6}$

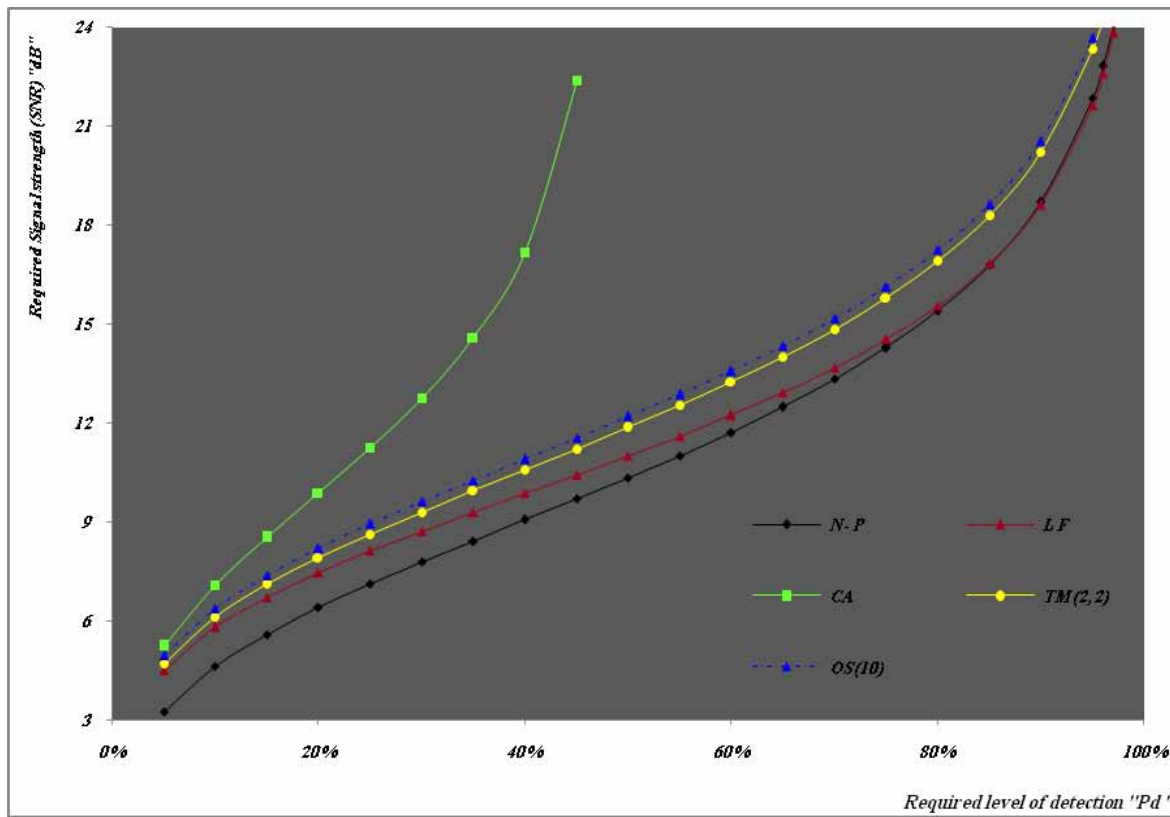


Fig. (8): M-sweeps multi-target signal strength requested to achieve a given level of detection of CFAR schemes for SWI target fluctuation model when  $N=24$ ,  $M=2$ ,  $R_1=R_2=1$ ,  $\theta=\gamma$ ,  $\rho_s=\rho_p$ , and  $P_{fa}=10^{-6}$

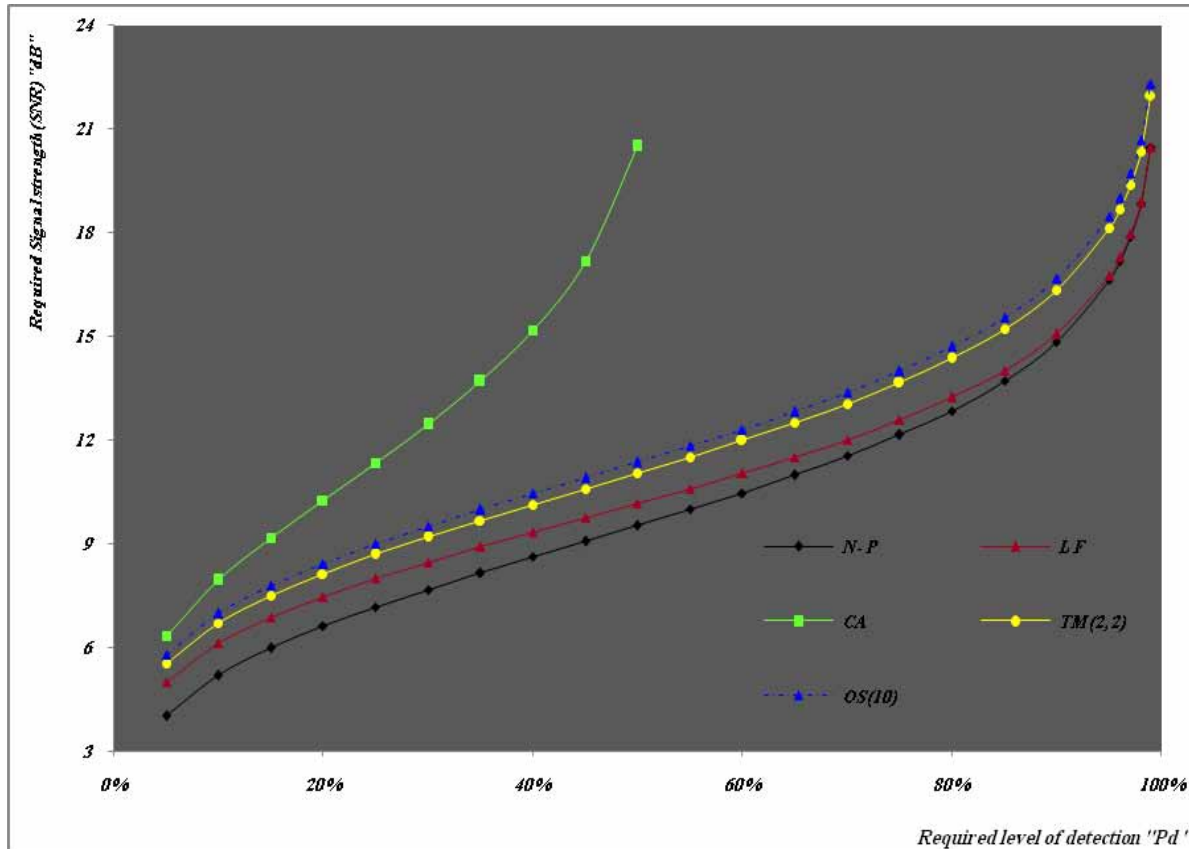


Fig. (9): M-sweeps multi-target signal strength requested to achieve a given level of detection of CFAR schemes for SWII target fluctuation model when  $N=24$ ,  $M=2$ ,  $R_1=R_2=1$ ,  $\theta=\gamma$ ,  $\rho_s=\rho_p$ , and  $P_{fa}=10^{-6}$

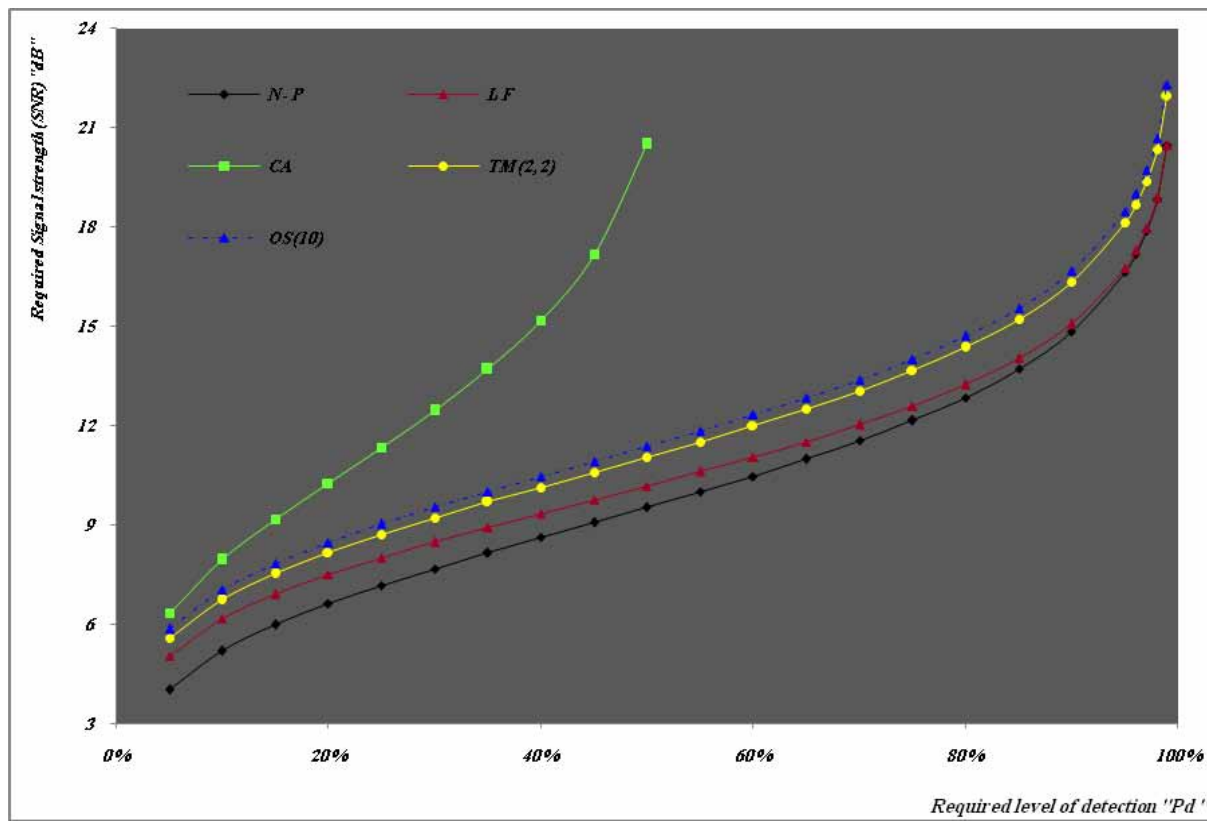


Fig. (10): M-sweeps multi-target signal strength requested to achieve a given level of detection of CFAR schemes for SWIII target fluctuation model when  $N=24$ ,  $M=2$ ,  $R=R=1$ ,  $\vartheta=\gamma$ ,  $\rho_s=\rho_p$ , and  $P_{fa}=10^{-6}$

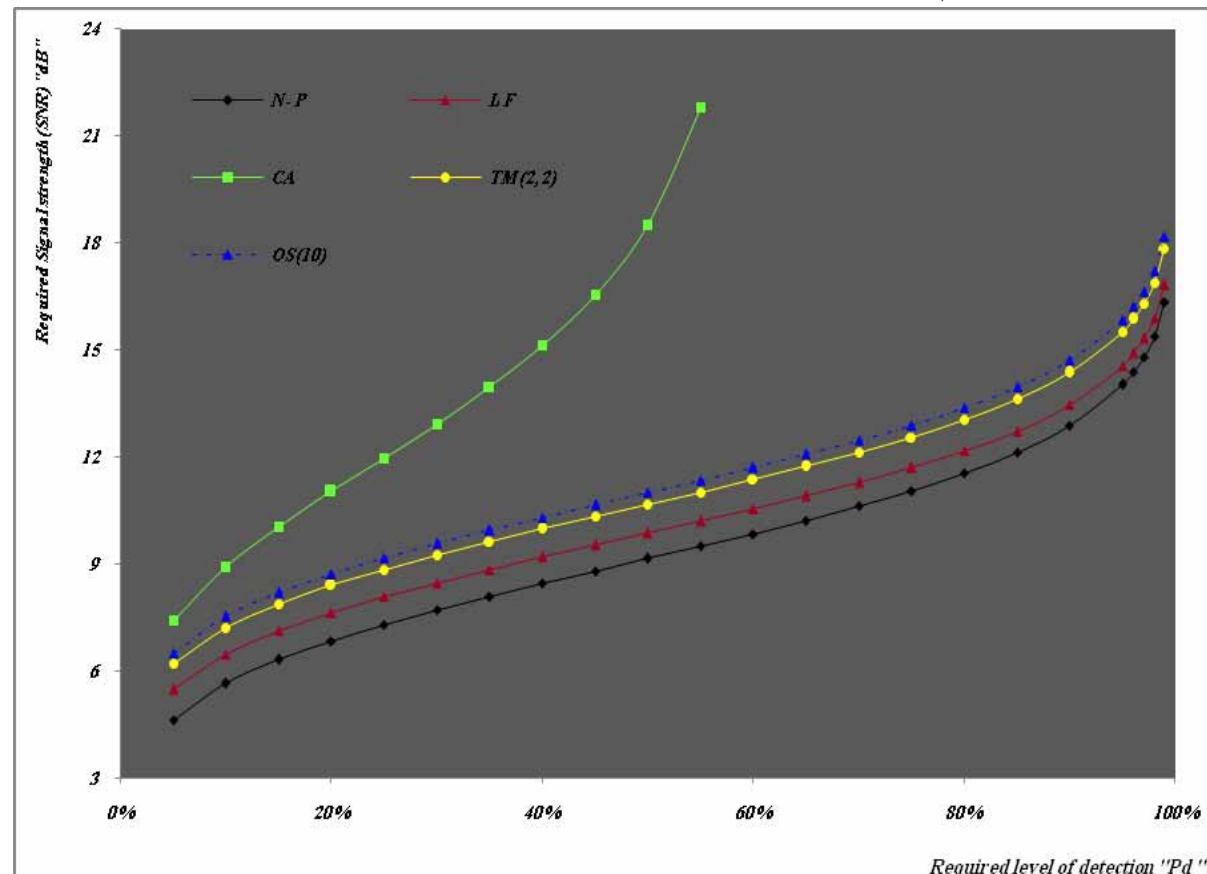


Fig. (11): M-sweeps multi-target signal strength requested to achieve a given level of detection of CFAR schemes for SWIV target fluctuation model when  $N=24$ ,  $M=2$ ,  $R_1=R_2=1$ ,  $\vartheta=\gamma$ ,  $\rho_s=\rho_p$ , and  $P_{fa}=10^{-6}$

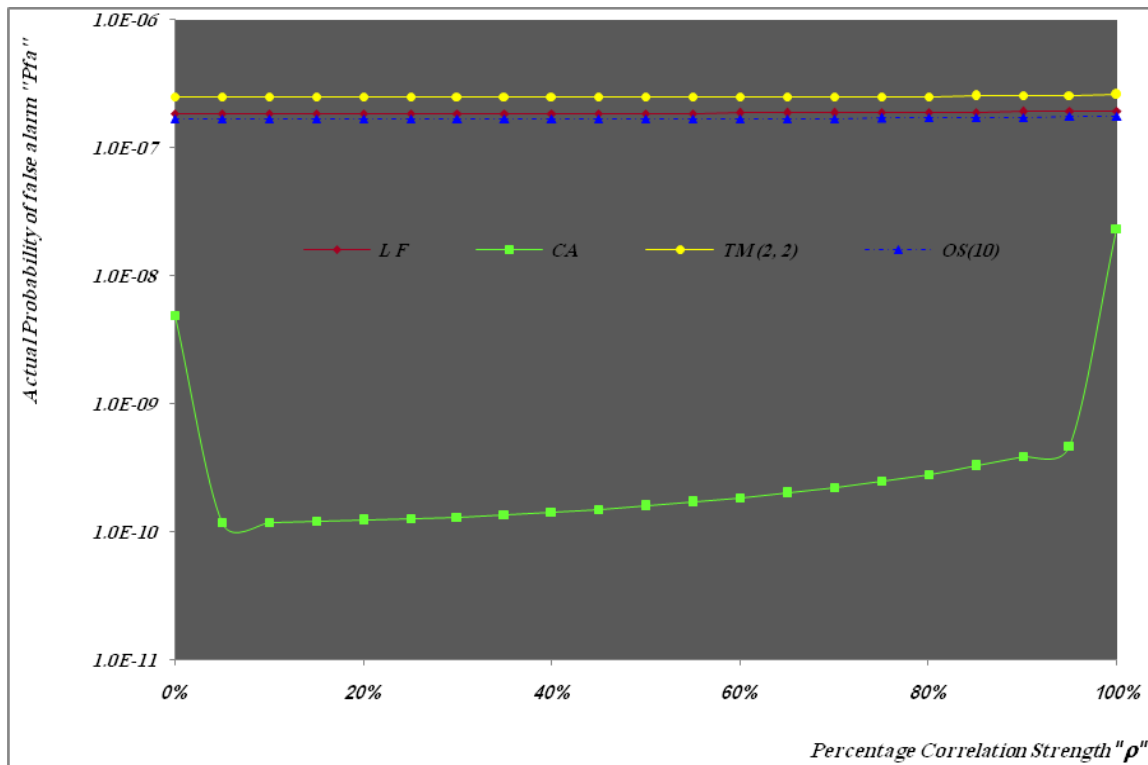


Fig. (12): M-sweeps multi-target actual false alarm performance of M-sweeps operation of CFAR detectors for two-degrees of freedom  $\chi^2$ -fluctuating targets when  $N=24$ ,  $M=2$ ,  $R_1=R_2=1$ ,  $\vartheta=10\text{dB}$ , and design  $P_{fa}=10^{-6}$

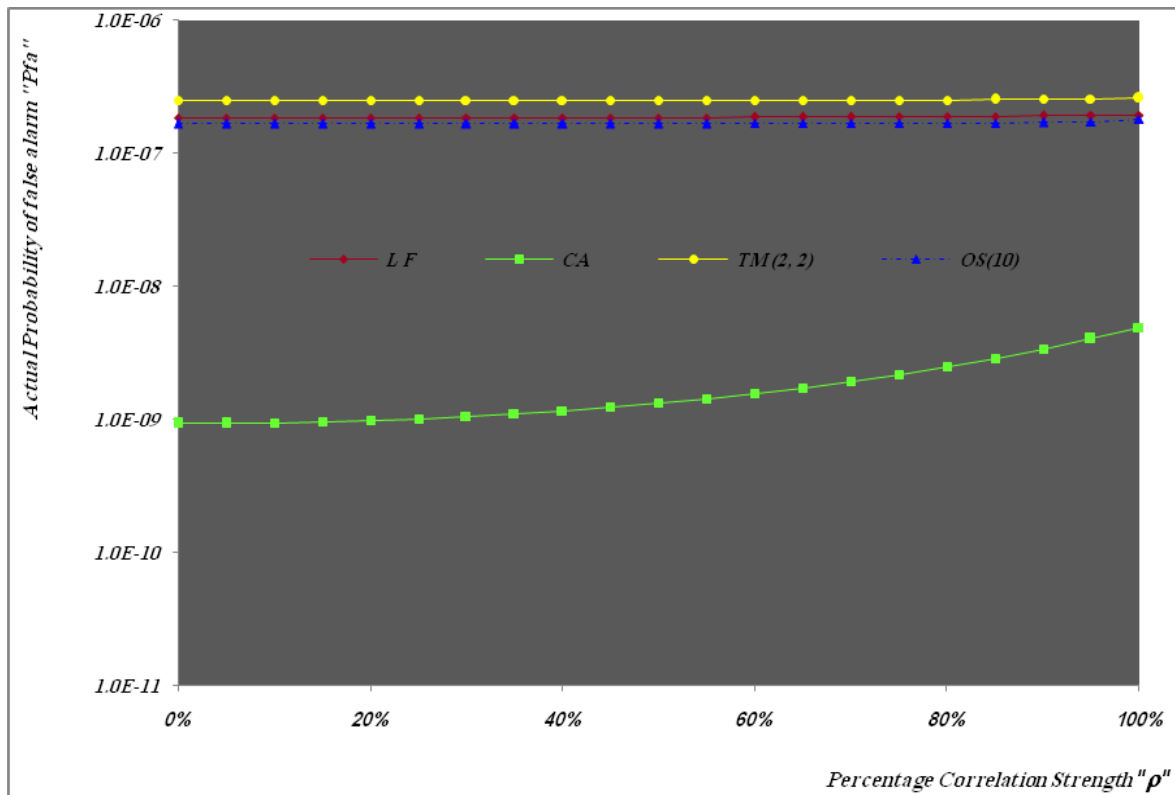


Fig. (13): M-sweeps multi-target actual false alarm performance of M-sweeps operation of CFAR detectors for four-degrees of freedom  $\chi^2$ -fluctuating targets when  $N=24$ ,  $M=2$ ,  $R_1=R_2=1$ ,  $\vartheta=10\text{dB}$ , and design  $P_{fa}=10^{-6}$